World Journal of Radiology

Submit a Manuscript: http://www.wjgnet.com/esps/
Help Desk: http://www.wjgnet.com/esps/helpdesk.aspx
DOI: 10.4329/wjr.v8.i1.21

World J Radiol 2016 January 28; 8(1): 21-49
ISSN 1949-8470 (online)

REVIEW

Diffusion-weighted magnetic resonance imaging in cancer: Reported apparent diffusion coefficients, *in-vitro* and *in-vivo* reproducibility

Maysam M Jafar, Arman Parsai, Marc E Miquel

Maysam M Jafar, Arman Parsai, Barts Cancer Institute, Queen Mary University of London, London E1 2AD, United Kingdom

Maysam M Jafar, Marc E Miquel, Clinical Physics, Barts Health NHS Trust, West Smithfield, London EC1A 7BE, United Kingdom

Arman Parsai, Radiology, Barts Health NHS Trust, West Smithfield, London EC1A 7BE, United Kingdom

Marc E Miquel, William Harvey Research Institute, Queen Mary University of London, London EC1M 6BQ, United Kingdom

Author contributions: All authors equally contributed to this paper with conception and design of the study, literature review and analysis, drafting and critical revision and editing, and final approval of the final version.

Conflict-of-interest statement: Authors declare no conflicts of interest for this paper.

Correspondence to: Maysam M Jafar, PhD, Clinical Physics, Barts Health NHS Trust, West Smithfield, London EC1A 7BE, United Kingdom. maysam.jafar@nhs.net
Telephone: +44-203-7658803
Fax: +44-203-4655785

Received: August 21, 2015
Peer-review started: August 24, 2015
First decision: September 30, 2015
Revised: November 10, 2015
Accepted: December 7, 2015
Article in press: December 8, 2015
Published online: January 28, 2016

Abstract

There is considerable disparity in the published apparent diffusion coefficient (ADC) values across different anatomies. Institutions are increasingly assessing repeatability and reproducibility of the derived ADC to determine its variation, which could potentially be used as an indicator in determining tumour aggressiveness or assessing tumour response. In this manuscript, a review of selected articles published to date in healthy extracranial body diffusion-weighted magnetic resonance imaging is presented, detailing reported ADC values and discussing their variation across different studies. In total 115 studies were selected including 28 for liver parenchyma, 15 for kidney (renal parenchyma), 14 for spleen, 13 for pancreatic body, 6 for gallbladder, 13 for prostate, 13 for uterus (endometrium, myometrium, cervix) and 13 for fibroglandular breast tissue. Median ADC values in selected studies were found to be 1.28 $\times 10^{-3}$ mm^2/s in liver, 1.94 $\times 10^{-3}$ mm^2/s in kidney, 1.60 $\times 10^{-3}$ mm^2/s in pancreatic body, 0.85 $\times 10^{-3}$ mm^2/s in spleen, 2.73 $\times 10^{-3}$ mm^2/s in gallbladder, 1.64 $\times 10^{-3}$ mm^2/s and 1.31 $\times 10^{-3}$ mm^2/s in prostate peripheral zone and central gland respectively (combined median value of 1.54$\times 10^{-3}$ mm^2/s), 1.44 $\times 10^{-3}$ mm^2/s in endometrium, 1.53 $\times 10^{-3}$ mm^2/s in myometrium, 1.71 $\times 10^{-3}$ mm^2/s in cervix and 1.92 $\times 10^{-3}$ mm^2/s in breast. In addition, six phantom studies and thirteen *in vivo* studies were summarized to compare repeatability and reproducibility of the measured ADC. All selected phantom studies demonstrated lower intra-scanner and inter-scanner variation compared to *in vivo* studies. Based on the findings of this manuscript, it is recommended that protocols need to be optimised for the body part studied and that system-induced variability must be established using a standardized phantom in any clinical study. Reproducibility of the measured ADC must also be assessed in a volunteer population, as variations are far more significant *in vivo* compared with phantom studies.

Key words: Diffusion-weighted magnetic resonance imaging; Apparent diffusion coefficient reproducibility; Apparent diffusion coefficient; Cancer imaging; Extra-cranial organs

Core tip: Diffusion-weighted magnetic resonance imaging was highlighted as a potential cancer imaging biomarker by a team of experts in a report published in 2009. We review the variability of published diffusion values in the major extra-cranial organs and focus on the validation literature, both *in vivo* and *in vitro*. A total of 115 studies were selected including for liver parenchyma, kidney, pancreatic body, spleen, gallbladder, prostate, uterus (endometrium, myometrium, cervix) and breast. We also look in detail at the published repeatability and reproducibility studies, both *in vivo* and in phantoms. A series of recommendations based on our findings are given at the end of this review.

Jafar MM, Parsai A, Miquel ME. Diffusion-weighted magnetic resonance imaging in cancer: Reported apparent diffusion coefficients, *in vitro* and *in vivo* reproducibility. *World J Radiol* 2016; 8(1): 21-49 Available from: URL: http://www.wjgnet.com/1949-8470/full/v8/i1/21.htm DOI: http://dx.doi.org/10.4329/wjr.v8.i1.21

INTRODUCTION

Diffusion-weighted magnetic resonance imaging (DW-MRI) was first implemented clinically in 1986[1] to study neurologic disorders. It has since developed into a mature technique for many brain applications[2]. In cancer imaging, DW-MRI has seen a great interest in both clinical and pre-clinical research during the past 20 years (with more than 106000 entries in Google Scholar for diffusion + mri + cancer). The concept of using DW imaging for the detection of malignant lesions started in early 1980s[3] but was not fully utilized until the late 1990s when a series of innovations in echo-planar imaging, high gradient amplitudes, multi-channel coils and parallel imaging made it possible to translate it to clinical settings[4]. DW-MRI was highlighted as a potential cancer imaging biomarker by a team of experts and stakeholders in a meeting report published in 2009[5]. In this report, it was also concluded that baseline patient reproducibility studies should be part of the study designs. After an introduction on the physics of diffusion weighted imaging, the article looks in more detail at what is actually measured *in vivo* and in particular the effect of perfusion as it has clear implications on the values measured using MRI. The article then reviews the variability of published diffusion values in the major extra-cranial organs and focuses on the validation literature, both *in vivo* and *in vitro*. Finally, DW-MRI reproducibility studies are summarized both using phantoms (6 studies) and *in vivo* (13 studies).

BASIC PRINCIPLES OF PULSED FIELD GRADIENT DW IMAGING

Diffusion is a Brownian motion of molecules in a medium[6]. At room temperature (298 K), a sample containing a small molecule, such as water, has a self-diffusion coefficient of about 2.3 × 10^{-3} mm^2/s[7]. In biologic tissues, diffusion coefficients are lower due to viscosity and restricted diffusion effects, which enables one to differentiate between different tissue structures[8]. Cellular tissues such as tumours often return lower diffusion values compared to healthy tissues, which facilitates their detection. In the presence of a magnetic field gradient, diffusion of water molecules causes a phase dispersion of the transverse magnetization, which results in the attenuation of the MRI signal[8]. In DW-MRI, image contrast is derived based on differences in the mobility of protons between tissues, which is reflected by the attenuation of the MRI signal. To increase the sensitivity to diffusion, all diffusion imaging pulse sequences contain a diffusion-weighting gradient.

Diffusion measurements are usually performed using a pulsed field gradient (PFG) pulse sequence. A spin-echo sequence is preferred as the 180° radio-frequency pulse refocuses chemical shifts and the frequency dispersion due to the residual B_0 inhomogeneity and susceptibility effects whilst a gradient echo only refocuses phase dispersion resulting from the gradient pulses[9]. Stejskal[10] and Tanner[11] introduced a PFG diffusion measurement method that uses two large gradient pulses with a short duration δ and separated by a variable time interval Δ as shown in Figure 1. In the presence of diffusion and gradient pulses, the attenuation due to relaxation and the attenuation due to diffusion and the applied gradient pulses are independent. This is expressed in equation (1.1).

$$S_b/S_0 = e^{-bD} \quad (1.1)$$

where S_b and S_0 are the voxel signal intensity with and without diffusion respectively and *b*-value controls the degree of diffusion weighting in an image and $b = \gamma^2 G^2 \delta^2 (\Delta - \delta/3)$ where γ is the gyromagnetic ratio and *G* is the amplitude of the diffusion gradients in mT/m.

Other pulse sequences, have been suggested to achieve diffusion-weighting, for example stimulated echo-based sequences[11,12] and steady-state free precession sequences[13-15].

Quantitative DW imaging is based on at least two DW images, each acquired at the same location but with a different *b*-value. A mono-exponential fit between the natural logarithm of the signal intensity of the tissue against the *b*-value is performed on a pixel-by-pixel basis and the slope of the linear regression yields the apparent diffusion coefficient (ADC) displayed in a

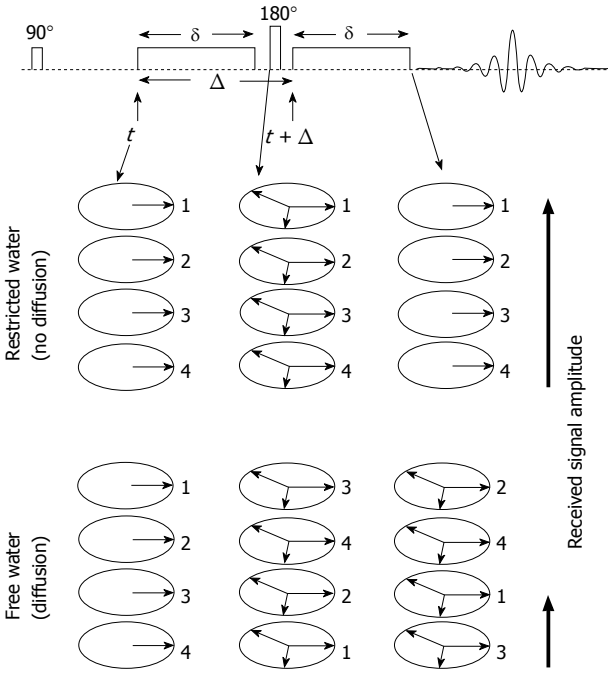

Figure 1 Schematic representation of the pulsed field gradient pulse sequence. In this description we assume that we start the sequence with a sample containing only four in-phase spins labelled with 1, 2, 3 and 4. In the absence of diffusion, the first gradient pulse causes dephasing of the spins. The 180° radio-frequency pulse reverses the sign of the phase angle and thus after the second gradient pulse all spins are in phase which gives a maximum echo signal. In the presence of diffusion, spins go through a random walk process resulting in a distribution of phases. This in turn results in poorer refocusing of the spins and thus, a smaller echo signal.

quantitative map. The calculated diffusion coefficient can be influenced by tissue perfusion and other experimental errors. Therefore, they are often referred to as ADCs. In practice, measurements in three orthogonal gradient directions are often obtained and the signals averaged, producing the corresponding *b*-value trace images[16]. Trace image S_D can be computed using a geometric average[17] of the DW images acquired in three orthogonal directions as expressed in equation (1.2). This is to average out the effects of anisotropy. The trace image is rotationally invariant which implies that image intensity is independent of patient orientation.

$$\langle S_D \rangle = (S_x.S_y.S_z)^{1/3} \quad (1.2)$$

Where $\langle S_D \rangle$ denotes the averaging process and S_x, S_y and S_z are the diffusion sensitizations acquired in three orthogonal directions. ADC maps are then computed from the isotropic diffusion image S_D and the baseline image S_0 (obtained without diffusion gradients) on a pixel-by-pixel basis using the relationship D = -ln (S_D/S_0)/*b*. This results in improvements in the signal to noise ratio of calculated ADC maps. The slope of the line that describes this relationship in each voxel represents the ADC. Despite using different scanner-specific techniques and image scaling methods to compute ADC maps, it was demonstrated that ADC measurements provided by different vendors were within 3% of the true value[18] using the diffusion coefficient of water at 0 ℃ as a reference.

DW IMAGING IN BIOLOGICAL TISSUE

In biological tissue, the DW signal is derived from the molecular diffusion of water and microcirculation of blood in the capillary network. In 1986, Le Bihan *et al*[1] proposed the principles of intravoxel incoherent motion (IVIM) to describe the microscopic translational motions that occur in each image voxel in DW imaging. The fraction of water diffusing and flowing in the capillaries of a given voxel involves only a fraction of total water content of the voxel[1,8]. This fractional volume is often referred to as the perfusion factor *f*. In all cases a biological tissue includes a volume fraction *f* of perfusion and a volume fraction 1 - *f* of diffusing water.

Hence equation (1.1) can be re-expressed as[1]:

$$S_b/S_0 = (1 - f)e^{-bD} + fe^{-b(D + D^*)} \quad (1.3)$$

where *D* is the diffusion coefficient of water molecules in the tissue and *D** is the fast pseudo-diffusion coefficient due to the incoherent flow of blood-water in the randomly oriented micro-vascular network. Microcirculatory perfusion of blood within capillaries depends on the velocity of the flowing blood and the vascular structure. Signal attenuation resulting from IVIM is typically an order of magnitude greater than tissue diffusion because of the larger distances of proton displacement during the application of the PFG pulses[19]. Therefore at higher *b*-values, IVIM accounts only for a small proportion of the measured signal in each imaging voxel. Experimental and clinical data indicate a bi-exponential behaviour of signal attenuation in body tissues using DW-MRI and this indicates that the signal attenuation observed at low *b*-values (< 100 s/mm^2) is related to tissue perfusion[1,5]. Other mathematical models have been suggested to describe quantitative DW-MRI namely stretched exponential[20], Gaussian[21] and Kurtosis[22].

A typical DW-MRI study in a patient whereby different images with multiple *b*-values are produced is shown in Figure 2. The range of *b*-values depends on investigator preferences and varies according to the anatomical region in the prospective study. The concept of a bi-exponential fit is also demonstrated in this figure.

The signal intensity from protons with larger diffusion distances per unit time such as blood flow is attenuated with small *b*-values (< 100 s/mm^2)[23]. This is in contrast to cellular tumours containing protons with shorter diffusion distances where there is usually less signal attenuation and hence higher *b*-values are required (> 500 s/mm^2)[23]. It has been shown that signal attenuation in liver DW-MRI is non-linear with increasing *b*-value due to microcapillary perfusion[24,25]. This can be seen clearly in Figure 2 where a bi-exponential fit (using the Levenberg-Marquardt algorithm) to the regions-of-interest (ROI) drawn on the DW-MR data acquired with

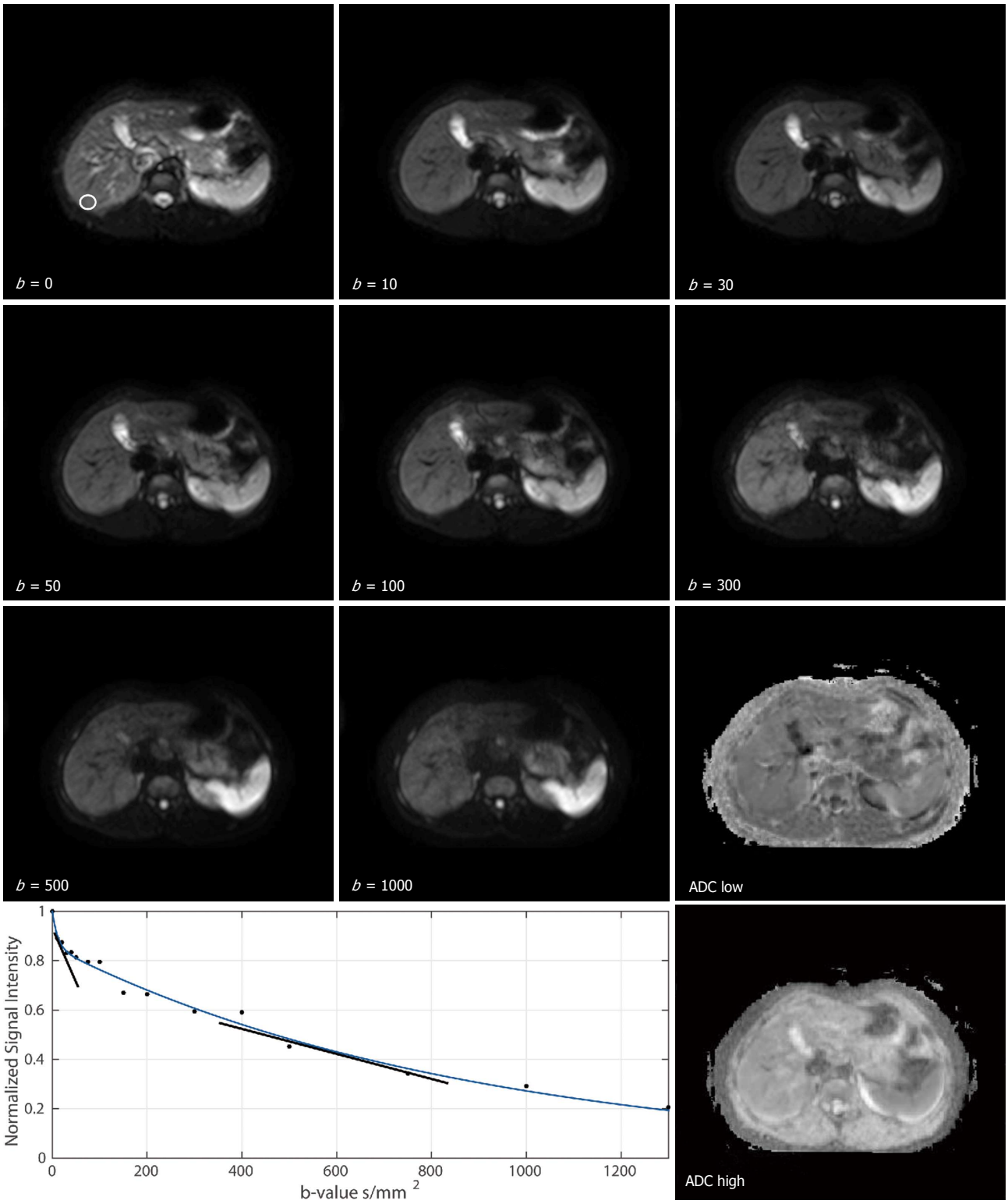

Figure 2 Diffusion-weighted magnetic resonance images of the abdomen of a healthy 25-year-old male volunteer at different *b*-values of 0, 10, 30, 50, 100, 300, 500, 1000 s/mm^2. An ROI placed over a non-heterogeneous region in the liver is shown on the b = 0 s/mm^2 image. A bi-exponential fit to the ROI drawn on the diffusion-weighted-magnetic resonance data acquired with *b*-values of 0, 10, 20, 30, 40, 50, 75, 100, 150, 200, 300, 400, 500, 750, 1000 and 1300 s/mm^2 is also shown where the slopes of the exponents represent the fast diffusion component (which includes perfusion) and the slower diffusion component. Quantitative apparent diffusion coefficients maps are also shown where ADC low was computed with *b*-values ≤ 100 s/mm^2 and ADC high was computed with *b*-values ≥ 150 s/mm^2. ROI: Region-of-interest; ADC: Apparent diffusion coefficient.

multiple *b*-values is shown. Whilst this is true for liver, in prostate DW-MRI a mono-exponential fit is sufficient to discriminate prostate cancer from normal tissue using *b*-values ranging from 0-800 s/mm^2[26] and that the perfusion component must be excluded in diagnosis, prognosis and treatment response[27]. Understanding the

IVIM[1,8] phenomenon is important because the choice of *b*-values determine the extent to which the computed ADC maybe influenced by tissue perfusion at low *b*-values. This explains why ADCs reported in abdominal studies using *b*-values (< 100 s/mm^2)[25,28-31] are higher than those obtained by using higher or a wide range of *b*-values[29,31-34].

"The signal intensity observed on the diffusion image is dependent on both water proton diffusivity and the tissue T_2-relaxation time"[23]. This means that a lesion may appear to show restricted diffusion on high *b*-value images due to long T_2-relaxation time rather than the limited mobility of water protons and are therefore difficult to characterize with visual assessment of DW-MR images[35]. This phenomenon is called T_2 shine-through effect and was first observed in brain diffusion imaging[36]. "The presence of T_2 shine-through is recognized by correlating high *b*-value images with the ADC map" whereby areas demonstrating T_2 shine-through rather than restricted diffusion will show "high diffusivity on the ADC map and high ADC values"[23].

"Water motion can occur preferentially in some directions in anisotropic tissues due to presence of obstacles that limit molecular movement in some directions"[23]. This anisotropic behaviour "can be detected by observing differences in diffusivity by using diffusion gradients in at least six directions". Diffusion tensor imaging has been used predominantly for brain imaging[37,38] with limited data for body imaging of liver[39,40], kidneys[41-43], breast[44] and prostate[45].

VARIABILITY OF PUBLISHED ADC VALUES IN NORMAL TISSUE

Most DW-MRI studies have been conducted using 1.5T MR systems although 3.0T systems are increasingly being used due to increased availability and potential for improved image quality[33,46-58]. The following sections are by no means a comprehensive review of all the published literature to-date but it is rather intended to give an overview of the variation in the published ADC values in clinical extra-cranial studies (*in vivo*) and provide the readers median values for the different organs. A total of 115 studies, were used in this review including for liver parenchyma, kidney (renal parenchyma), pancreatic body, spleen, gallbladder, prostate, uterus (endometrium, myometrium, cervix) and breast. These studies were selected using Google as the search engine where selection was based on highly cited detailed articles in the relevant anatomy. Healthy tissue investigator reports in anatomies such as uterus and gallbladder are noticeably less compared with that of liver and therefore studies with a low number of citations were also included. Recent reports (those published in 2015) were selected using Google Scholar by applying the date filter. In the selection of all of these studies, different magnet field strengths from different vendors, a wide range of *b*-values, a number of different diffusion sequences and different human populations from different regions and continents were included. This was to remove vendor-specific, sequence-specific and population-specific bias. Box and whisker plots for the different organs are shown in Figure 3. Details of the studies are provided in, Tables 1-8.

Liver

In DW-MR literature, no organ in the abdomen has received more attention than the liver[46]. Several investigators have reported the usefulness of DW-MRI for detection of malignant liver lesions[24,28,47]. Ichikawa *et al*[28] found that DW-MR differentiated between hemangiomas, hepatocellular carcinomas (HCCs) and metastases and that their respective mean ADC values were significantly greater than the mean ADC values of the normal liver. Liver DW-MRI is routinely performed by using tri-directional diffusion gradients along each of the x, y and z directions[23]. Reported ADC values in healthy liver parenchyma (Table 1) vary between 0.81 ± 0.09 × 10^{-3} mm^2/s[48] to 2.4 ± 0.5 × 10^{-3} mm^2/s[49] leading to a median value of 1.28 × 10^{-3} mm^2/s. Values are reportedly higher in studies where *b*-values of less 100 s/mm^2 were solely used in the computation of the ADC[28,29] due to perfusion effects. Insignificant differences in ADC values between the three diffusion gradient directions were observed[47], proving the isotropic structure of liver parenchyma. Because of the relatively short T_2-relaxation time of the normal liver parenchyma, 46 ± 6 ms at 1.5T and 34 ± 4 ms at 3.0T[50], the *b*-values used in clinical imaging are typically no higher than 1000 s/mm^2[23] although some studies did use *b*-values of up to 1300 s/mm^2[32]. To generate higher *b*-values longer PFG pulses with longer echo times are needed and therefore loss of signal from T_2 decay. The ideal TE in DW-imaging of extra-cranial organs should approximately be the T_2-relaxation time of the organ undergoing the study. Some studies looking at DW imaging of the liver used TE values significantly higher than the T_2-relaxation time[24,47]. In liver DW-MRI, only few studies are known that have used a TE of less than 50 ms[33,51]. Taouli and Koh[23] suggested a minimum echo time of 71 ms to reduce shine-through effect, which should be kept fixed for all *b*-values used in the study. They also recommended *b*-values of less than 500 s/mm^2 for breath-hold acquisitions and less than 1000 s/mm^2 for free breathing or respiratory triggered acquisitions. DW-MR combined with T_1-weighted and T_2-weighted imaging was shown to perform equally as well as Gadolinium-MR in the diagnosis of liver metastases[52]. Guo *et al*[53] found that a correlation exists between ADC values and the histological grade of HCCs although some HCCs were poorly differentiated due to overlap of ADC values with those of normal liver. These findings were contrary to the report by Nasu *et al*[54] whereby no correlation was found between ADC values and the histological grade of HCCs. This discrepancy in findings could be attributed to the placement of ROIs where the investigators in[54] defined ROIs encompassing HCCs in their entirety whereas necrotic and hemorrhagic areas

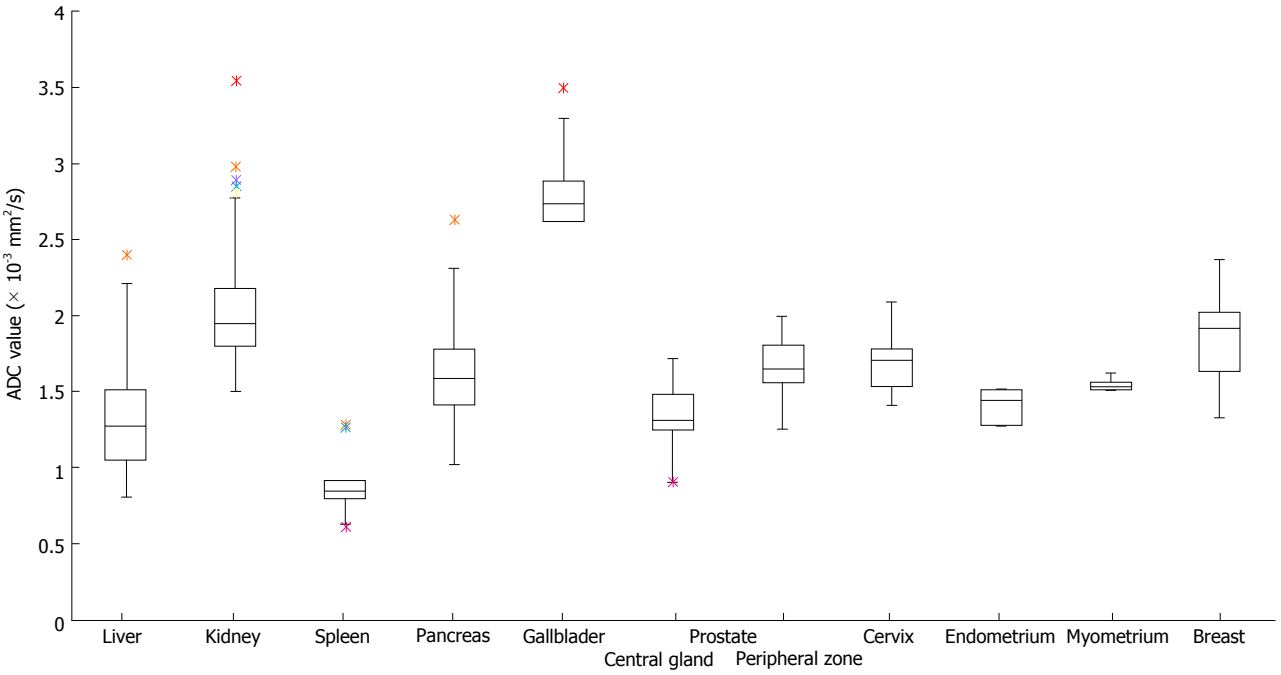

Figure 3 Box and whisker plots of the summarised apparent diffusion coefficient values reported for extra-cranial organs. A total of 115 studies were summarised including for liver parenchyma, kidney (renal parenchyma), pancreatic body, spleen, gallbladder, prostate (peripheral zone and central gland), uterus (endometrium, myometrium, cervix) and breast. Details of the studies are provided in Tables 1-8. ADC: Apparent diffusion coefficient.

were deliberately avoided by the investigators in[53].

Kidney

The major role of the kidneys is water reabsorption and concentration-dilution functions[41] and, therefore, DW-MRI may provide useful insights into the mechanisms of various renal diseases. The majority of published values in renal parenchyma DW-MRI (Table 2) report an ADC estimate for two tissue types, renal cortex (outer portion of the kidney) and renal medulla (innermost part of the kidney)[30,31,55,56]. Some studies reported ADC values for the left and right kidneys with statistically insignificant difference between the two values[57,58]. Few studies reported anisotropic diffusion in the kidney particularly in the renal medulla due to the radial orientation of the renal vessels and the collecting system[41,59]. The T_2-relaxation time in renal cortex and renal medulla are 87 ± 4 ms and 85 ± 11 ms at 1.5T and 76 ± 7 ms and 81 ± 8 ms at 3.0T respectively[50]. The highest ADC estimate across the entire kidney (3.54 ± 0.47 × 10^{-3} mm^2/s) was reported in[60] where the authors used an echo time of 18 ms achieved by having a stimulated-echo DW-MR sequence and *b*-values of less than 400 s/mm^2. Other authors[29,31] did report ADC estimates of higher than 3.70 × 10^{-3} mm^2/s but the *b*-values used in the computation were less than 150 s/mm^2 and therefore, perfusion effects led to an increase in the computed ADC value. ADC values in selected studies varied between 1.50 × 10^{-3} mm^2/s [31] and 3.54 × 10^{-3} mm^2/s[60] leading to a median value of 1.94 × 10^{-3} mm^2/s.

Spleen

Normal spleen as well as accessory spleens, have the greatest degree of non-pathological restricted diffusion of all solid abdominal organs[61]. In DW-MRI of healthy spleen tissue (Table 3), the highest computed ADC in the selected studies was 1.28 ± 0.39 × 10^{-3} mm^2/s[49] using *b*-values of ≤ 400 s/mm^2 while the lowest was 0.59 ± 0.04 × 10^{-3}[32] using *b*-values of ≤ 1300 s/mm^2 leading to a median value of 0.85 × 10^{-3} mm^2/s. Several authors have proposed to use the spleen as a reference organ for ADC measurements of liver parenchyma[29,62] in order to decrease variability of liver ADC measurements despite the fact that patients with cirrhosis and portal hypertension frequently suffer from splenomegaly (enlargement of the spleen)[63]. Klasen *et al*[63] demonstrated that patients with liver cirrhosis and portal hypertension had significantly higher spleen ADCs. Spleen T_2-relaxation times are 79 ± 15 ms and 61 ± 9 ms at 1.5T and 3.0T respectively[50] and some studies[24,64] did use echo times significantly higher than the T_2-relaxation time.

Pancreas

Evaluation of solid lesions in the pancreas lies mainly in the discrimination between benign mass-forming focal pancreatitis and pancreatic carcinoma[65]. Unfortunately differentiating between benign mass-forming focal pancreatitis and pancreatic ductal adenocarcinoma is extremely difficult as they both show similar histologic and radiologic patterns[66-68]. Multimodality approaches such as ultrasound, computed tomography and different MR techniques have been suggested to differentiate between benign mass-forming focal pancreatitis and pancreatic carcinoma[66]. Healthy pancreatic tissue ADC

Table 1 Estimates of apparent diffusion coefficient values reported in healthy human liver using a mono-exponential fit

Ref.	System	Field strength (T)	Sequence	TR/TE (ms/ms)	No. of patients/mean age (SD) (yr)	*b*-values (s/mm^2)	Mean ADC (SD) (× 10^{-3} mm^2/s)
Müller *et al*[60], 1994	Siemens	1.5	STEAM EPI, BH	2BH/18	10 (7F, 3M)/24	2, 8, 22, 32, 57, 89, 176, 395	1.39 (0.16)
Ichikawa *et al*[28], 1998	Siemens Vision	1.5	SS SE EPI, BH, FS	NR/54	46 (14F, 32M)/58	1.6, 16, 55	2.28 (1.23)
Yamada *et al*[24], 1999	Siemens Vision	1.5	SS SE EPI, BH, FS	NR/123	47	0, 30, 300, 900, 1100	0.87 (0.26)
Kim *et al*[29], 1999	GE Signa	1.5	SS SE EPI, BH (6s), FS	NR/70	P1: 6 (1F, 5M)/29 P2: 48 (18F, 30M)/57	3, 57, 192, 408, 517, 705, 846	*b* < 850: P1: 1.05 (0.30) P2: 1.02 (0.25) *b* < 410: P1: 1.55 (0.37) P2: 1.16 (0.42) *b* < 100: P1: 4.80 (2.37) P2: 3.55 (1.75)
Moteki *et al*[25], 2002	Siemens Impact	1.0	Turbo FLASH, BH, FA = 12°	8.8/4	46	0, 50.2, 295	1.11 (1.02), 12.3 (5.17)
[1]Mürtz *et al*[52], 2002	Philips Intera	1.5	SS EPI, RT, BHE, SPIR + four saturation slabs	(1) RT, 4HB/83 (2) 3000/83	12 (4F, 8M)/31	50, 300, 700, 1000, 1300	(1) 0.92-0.96 (0.09-0.14) (2) 1.03-1.14 (0.22-0.40)
Boulanger *et al*[155], 2003	GE Signa	1.5	SS EPI, BH	3000/52	10 (2F, 8M)/43.5	50, 100, 150, 200, 250	1.79 (0.25)
Chow *et al*[55], 2003	GE Signa	1.5	SS EPI	3000/(46.9-57.5)	12 (4F, 8M)/29	10, 300	1.697 (0.052)
Taouli *et al*[47], 2003	Philips Intera	1.5	SS EPI, BH, FS	(1) 2400/ 104 (2) 3106/ 104	14	(1) 0, 500 (2) 0, 134, 267, 400	(1) 1.83 (0.36) (2) 1.51 (0.49)
Taouli *et al*[39], 2004	Philips Intera	1.5	SS EPI, FS	(1800-2400)/(63-83)	10 (3F, 7M)/33	0, 500	NPI: 1.60 (0.13) PI: 1.52 (0.15) DTI + PI: 1.51 (0.21)
Deng *et al*[156], 2006	Siemens Sonata	1.5	(1) SS SE EPI, BH (2) MS PROPELLER, FB, RT, FS + 2 saturation slabs	2000/82 2000/105	9	0, 502	(1) 1.18 (0.14) (2) 1.39 (0.19)
Lewin *et al*[157], 2007	Siemens Maestro	1.5	SS SE EPI, NC, FS	1400/76	20 (9F, 11M)/31.4 (7)	0, 200, 400, 800	1.44 (0.02)
Taouli *et al*[158], 2007	Siemens Avanto	1.5	SS EPI, BH, FS	1300/(51-71)	7 (2F, 5M)/32	0, 50, 300, 500, 700, 1000	1.66 (0.12)
Luciani *et al*[159], 2008	Siemens Avanto	1.5	RT	1500/70	25 (13F, 12M)/48 (16)	0, 200, 400, 800	1.39 (0.2)
Bruegel *et al*[160], 2008	Siemens Avanto	1.5	SS EPI, NC, BH, FS	NR/69	102 (46F, 56M)/61	50, 300, 600	1.24 (0.15)
Braithwaite *et al*[49], 2009	Siemens Trio	3.0	Stimulated echo EPI, FB, FS	3200/76	20 (20M)/34.7	0, 400	2.4 (0.50) E
[2]Saremi *et al*[161], 2011	a. Siemens Avanto b. Siemens Trio	a. 1.5 b. 3.0	SS SE EPI, FS (1) BH, no PI (2) BH, PI (3) FB, PI	(1) 150/75 (2) 144/72 (3) 174/87	13 (2F, 11M)/46 (13)	50, 400, 1000	a. 0.86(0.2) b. 0.83(0.2)
Watanabe *et al*[51], 2011	Philips Achieva	3.0	SS EPI, BH	2291/44	18	0, 500	1.36 (0.11)
Bakan *et al*[162], 2012	Siemens Avanto	1.5	SS SE EPI, FS	4800/82	25 (11F, 14M)/39.8 (11.4)	0, 500, 1000	1.75 (0.14)
Miquel *et al*[34], 2012	Philips Achieva	1.5	SS SE EPI, FB	(5300-5800)/62	10 (7F, 3M)/32.3 (4.6)	100, 200, 500, 750, 1000	V1: 1.05 (0.04) V2: 1.06 (0.07)
[3]Andreou *et al*[163], 2013	Siemens Avanto	1.5	SS SE EPI, NC, RT, FS	5000/68	14 (7F, 7M)/59.7	0, 25, 50, 75, 100, 250, 500, 900	1.22
Corona-Villalobos *et al*[58], 2013	Siemens Avanto	1.5	SS SE EPI, BH	(1) 3000/(69-79) (2) 2500/(76-95)	100 (36F, 64M)/60.4 (14.3)	(1) 0, 750 (2) 0, 50, 100, 200, 300, 450, 600, 750	(1) 1.22 (0.15) (2) 0.96 (0.08)

Klasen *et al*[63], 2013	Siemens Avanto	1.5	SS EPI	(6825-6930)/(68-76)	50 (30F, 20M)/55.1	50, 300, 600	O1: 1.053 (0.124) O2: 1.088 (0.146)
Larsen *et al*[48], 2013	Philips Achieva	3.0	SS SE EPI, BHI, BHE, RT, FB, FS	(1600-2000)/71-72	10 (4F, 6M)/24	0, 150, 500, 750, 1000	*b* = 0, 750: BHI: 1.52 (0.11) BHE: 1.54 (0.1) FB: 1.44 (0.11) RT: 1.48 (0.11) *b* = 150, 750: BHI: 0.81 (0.09) BHE: 0.83 (0.10) FB: 0.91 (0.08) RT: 0.92 (0.07)
Penner *et al*[164], 2013	Philips Intera	1.5	SS SE EPI, RT, SPIR	1648/63	15 (12F, 3M)/44 (11)	0, 50, 800	1.30 (0.11)
Donati *et al*[56], 2014	(1) Siemens Sonata (2) Siemens Trio (3) Philips Achieva (4) Philips Achieva (5) GE Signa (6) GE Discovery	1.5 3.0 1.5 3.0 1.5 3.0	SS SE EPI, FB, FS	(5000-6225)/(36-76)	10 (10M)/36.6 (7.7)	0, 1000	(1) LL: 1.207 (0.194) RL: 1.026 (0.260) (2) LL: 1.132 (0.250) RL: 0.966 (0.187) (3) LL: 1.349 (0.178) RL: 1.128 (0.127) (4) LL: 1.097 (0.129) RL: 1.108 (0.110) (5) LL: 1.271 (0.133) RL: 1.151 (0.162) (6) LL: 1.524 (0.356) RL: 1.280 (0.372)
Leporq *et al*[33], 2015	GE Discovery	3.0	SE EPI, RT, FB, No FS	2000/(48-55)	25 (9F, 16M)/27.1 (4.5)	0, 800	RT: 1.65 (0.28) FB + (TE = 48): 1.63 (0.22) FB + (TE = 55): 1.57 (0.26) FB + WA: 1.55 (0.24)
Duran *et al*[165], 2015	Philips Intera	1.5	SS EPI, FB, SPIR	3448/63	53 (33F, 20M)/50	0, 150, 600	1.52 (0.32)

Some studies were carried out with more *b*-values than specified in the following table to compute IVIM-specific parameters. [1]Range for three diffusion directions; [2]Mean ADC of the three sequences reported in the paper; [3]These authors reported the mean of median ADC values. ADC: Apparent diffusion coefficient; F: Female; M: Male; NR: Not reported; SS: Single shot; MS: Multi-shot; SE: Spin echo; STEAM: Stimulated echo; EPI: Echo planar imaging; RF: Radiofrequency; RT: Respiratory triggered; NC: Navigator controlled; FB: Free breathing; BH: Breath-hold; BHI: Breath-hold end inspiratory; BHE: Breath-hold end expiratory; SPIR: Spectral pre-saturation with inversion recovery; FS: Fat suppressed; E: Estimated from the chart; FA: Flip angle; P: Population; V: Visit; PI: Parallel imaging; NPI: No parallel imaging; DTI: Diffusion tensor imaging; WA: Weighted averaging for different *b* values; LL: Left liver lobe; RL: Right liver lobe.

estimates (Table 4), range between 1.02 ± 0.28 × 10^{-3} mm^2/s[24] to 2.63 ± 0.72 × 10^{-3} mm^2/s[49] leading to a median value of 1.60 × 10^{-3} mm^2/s. Estimated ADC values were shown to be statistically insignificant between normal pancreatic tissue, benign mass-forming focal pancreatitis and pancreatic carcinoma[65]. Ichikawa *et al*[69] demonstrated that qualitative high *b*-value DW-MRI is valuable in detecting pancreatic carcinomas and may prove more useful than a quantitative measure such as the computed ADC. It has been suggested that DW-MRI of the pancreas should act as a supplement to other imaging modalities to differentiate between benign mass-forming focal pancreatitis

Table 2 Estimates of apparent diffusion coefficient values reported in human kidney (renal parenchyma) using a mono-exponential fit

Ref.	System	Field strength (T)	Sequence	TR/TE (ms/ms)	No. of patients/mean age (SD) (yr)	*b*-values (s/mm^2)	Mean ADC (SD) (× 10^{-3} mm^2/s)
Müller *et al*[60], 1994	Siemens	1.5	STEAM EPI, BH	2BH/18	10 (7F, 3M)/24	2, 8, 22, 32, 57, 89, 176, 395	3.54 (0.47)
Kim *et al*[29], 1999	GE Signa	1.5	SS SE EPI, BH (6s), FS	NR/70	P1: 6 (1F, 5M)/29 P2: 48 (18F, 30M)/57	3, 57, 192, 408, 517, 705, 846	b < 850: P1: 1.79 (0.27) P2: 1.92 (0.32) *b* < 410: P1: 1.79 (0.49) P2: 2.14 (0.44) *b* < 100: P1: 2.98 (3.01) P2: 3.73 (1.94)
Yamada *et al*[24], 1999	Siemens Vision	1.5	SS SE EPI, BH, FS	NR/123	78	0, 30, 300, 900, 1100	1.55 (0.27)
Namimoto *et al*[30], 1999	Siemens Vision	1.5	SS SE EPI, BH	NR/123	16	30, 300	M: 2.84 (0.72) C: 2.55 (0.62)
Ries *et al*[41], 2001	Philips	1.5	(1) SS EPI, BH (2) MS EPI, BH	BH/86 BH/94	10	0, 195, 390	a. C: 2.80 (0.32) M: 2.30 (0.42) b. C: 2.89 (0.28) M: 2.18 (0.36)
[1]Mürtz *et al*[32], 2002	Philips Intera	1.5	SS EPI, RT, BHE, SPIR + four saturation slabs	(1) RT, 4HB/83 (2) 3000/83	12 (4F, 8M)/31	50, 300, 700, 1000, 1300	C: (1) 1.63-1.66 (0.09-0.14) (2) 1.67-1.81 (0.22-0.26)
Chow *et al*[55], 2003	GE Signa	1.5	SS EPI	3000/(46.9-57.5)	12 (4F, 8M)/29	10, 300	M: 2.091 (0.055) C: 2.58 (0.053)
Thoeny *et al*[31], 2005	Siemens Sonata	1.5	SS EPI, FB, FS + two saturation slabs	3200/71	18 (5F, 13M)/27	0, 50, 100, 150, 200, 250, 300, 500, 750, 1000	*b* ≤ 1000: M: 1.87 (0.08) C: 2.03 (0.09) *b* > 300: M: 1.50 (0.12) C: 1.67 (0.11) *b* < 150: M: 3.76 (0.55) C: 3.72 (0.45)
Yoshikawa *et al*[57], 2006	Philips Intera	1.5	SS EPI, BH, SPIR	1500/66	(1) 145 (2) 144	0, 600	(1) R, 2.67 (0.29) (2) L, 2.60 (0.32)
Kilickesmez *et al*[64], 2008	Siemens Avanto	1.5	SS EPI, FB, FS	4900/93	50 (29F, 21M)/38.9	0, 500, 1000	M: 1.94 (0.18) C: 2.08 (0.22)
[2]Saremi *et al*[161], 2011	a. Siemens Avanto b. Siemens Trio	a. 1.5 b. 3.0	SS SE EPI, FS (1) BH, no PI (2) BH, PI (3) FB, PI	(1) 150/75 (2) 144/72 (3) 174/87	13 (2F, 11M)/46 (13)	50, 400, 1000	a. 1.8 (0.1) b. 1.8 (0.1)
Miquel *et al*[34], 2012	Philips Achieva	1.5	SS SE EPI, FB	(5300-5800)/62	10 (7F, 3M)/32.3 (4.6)	100, 200, 500, 750, 1000	V1: 1.76 (0.08) V2: 1.76 (0.10)
Corona-Villalobos *et al*[58], 2013	Siemens Avanto	1.5	SS SE EPI, BH	(1) 3000/(69-79) (2) 2500/(76-95)	100 (36F, 64M)/60.4 (14.3)	(1) 0, 750 (2) 0, 50, 100, 200, 300, 450, 600, 750	(1) R, 2.07 (0.18) L, 2.08 (0.19) (2) R, 1.79 (0.17) L, 1.78 (0.16)
Donati *et al*[56], 2014	(1) Siemens Sonata	1.5	SS SE EPI, FB, FS	(5000-6225)/(36-76)	10 (10M)/36.6 (7.7)	0, 1000	(1) C: 1.92 (0.169)

	(2) Siemens Trio						M: 1.90 (0.137)
	(3) Philips Achieva	3.0					(2) C: 1.86 (0.132)
	(4) Philips Achieva						M: 1.80 (0.093)
	(5) GE Signa	1.5					(3) C: 1.95 (0.176)
	(6) GE Discovery						M: 1.93 (0.11)
		3.0					(4) C: 1.94 (0.132)
							M: 1.90 (0.11)
		1.5					(5) C: 1.95 (0.156)
		3.0					M: 1.94 (0.143)
							(6) C: 2.05 (0.194)
							M: 1.93 (0.147)
Sulkowska *et al*[166], 2015	Philips Ingenia	1.5	SS EPI	NR/71	50 (28F, 22M)/39 (12)	(1) 0, 50, 100, 150, 200, 250, 300, 350, 400, 450, 500, 550, 600, 650, 700, 750	(1) C: 2.26 (0.2) M: 2.21 (0.17)
						(2) 0, 10, 20, 40, 60, 150, 300, 500, 700, 900	(2) C: 2.13 (0.16) M: 2.06 (0.2)

Some studies were carried out with more *b*-values than specified in the following table to compute intravoxel incoherent motion-specific parameters. [1]Range of values for three directions; [2]Mean ADC of the three sequences reported in the paper. ADC: Apparent diffusion coefficient; F: Female; M: Male; NR: Not reported; SS: Single shot; MS: Multi-shot; SE: Spin echo; STEAM: Stimulated echo; EPI: Echo planar imaging; RF: Radiofrequency; RT: Respiratory triggered; NC: Navigator controlled; FB: Free breathing; BH: Breath-hold; BHI: Breath-hold end inspiratory; BHE: Breath-hold end expiratory; SPIR: Spectral pre-saturation with inversion recovery; FS: Fat suppressed; E: Estimated from the chart; FA: Flip angle; P: Population; V: Visit; PI: Parallel imaging; NPI: No parallel imaging; DTI: Diffusion tensor imaging; WA: Weighted averaging for different *b* values; LL: Left liver lobe; RL: Right liver lobe.

and pancreatic carcinoma[65,70]. Pancreatic tissue T_2-relaxation times are 46 ± 6 ms and 43 ± 7 ms at 1.5T and 3.0T respectively[50]. Barral *et al*[70] recommended the use of DW-MRI where there is a clinical suspicion and imaging findings suggestive of endocrine pancreatic tumour as well as for the detection of liver metastasis in patients with exocrine pancreatic tumours. Multi-centre studies of the DW-MRI of the pancreas in terms of image quality and reproducibility of the diffusion parameters are needed to assess the suitability of ADC in the evaluation of pancreatic disease[70]. Nevertheless, DW-MRI of the pancreas will have an expanded role in the evaluation of patients with pancreatic disease since technological advancements continue to improve the quality of clinical DW-MRI[70].

Gallbladder

Ultrasonography is usually the modality of choice in evaluating gallbladder diseases[71] because of its relatively low cost and widespread availability. DW-MRI is more widely used for further characterisation of potentially malignant gallbladder lesions. Limited DW-MRI data exist for gallbladder as T_2-weighted MRI in the biliary tracts is generally used to assess the extent of disease and cancer staging[72].

Healthy gallbladder ADC estimates reported in selected studies are shown in Table 5. Reported ADC estimates of the gallbladder in the selected studies range between $2.506 \pm 0.223 \times 10^{-3}$ mm^2/s[56] and $3.50 \pm 0.51 \times 10^{-3}$ mm^2/s[57] leading to a median value of 2.73×10^{-3} mm^2/s. As a reference point, the diffusion coefficient of water at 35 ℃ is 2.92×10^{-3} mm^2/s[7] and correcting for c.a. 2.4% variation per degree Celsius change in temperature[73] yields 3.06×10^{-3} mm^2/s at 37 ℃ body temperature. All ROIs in the selected studies were placed over the biliary liquid encompassed by the gallbladder. Placement of ROIs differed by investigators and none of them discussed partial volume effects, which could potentially alter the ADC estimate due to ROI placement over the gallbladder wall. Size of ROIs differed among investigators ranging from an oval 100 mm^2[57], to a 32 pixel ROI[56] placed at the centre of the gallbladder (average pixel size 3.125 mm), to an ROI encompassing the entire gallbladder[34] and finally, to an ROI standardized to 2 cm^2[58]. The effect of T_2 shine-through can be seen clearly in the normal gallbladder and most studies used *b*-values of up to 1100 s/mm^2. Yamada *et al*[24] found that the perfusion fraction in gallbladder is zero and that diffusion is the only type of motion in gallbladder on a par with ascites.

Table 3 Estimates of apparent diffusion coefficient values reported in human spleen using a mono-exponential fit

Ref.	System	Field strength (t)	Sequence	TR/TE (ms/ms)	No. of patients/mean age (sd) (yr)	*b*-values (s/mm^2)	Mean ADC (sd) (× 10^{-3} mm^2/s)
Müller *et al*[60], 1994	Siemens	1.5	STEAM EPI, BH	2BH/18	10 (7F, 3M)/24	2, 8, 22, 32, 57, 89, 176, 395	0.95 (0.15)
Yamada *et al*[24], 1999	Siemens Vision	1.5	SS SE EPI, BH, FS	NR/123	76	0, 30, 300, 900, 1100	0.88 (0.33)
Kim *et al*[29], 1999	GE Signa	1.5	SS SE EPI, BH (6sec), FS	NR/70	P1: 6 (1F, 5M)/29 P2: 48 (18F, 30M)/57	3, 57, 192, 408, 517, 705, 846	*b* < 850: P1: 0.93 (0.30) P2: 0.80 (0.34) *b* < 410: P1: 0.85 (0.25) P2: 0.99 (0.54) *b* < 100: P1: 2.17 (3.28) P2: 2.81 (1.93)
[1]Mürtz *et al*[32], 2002	Philips Intera	1.5	SS EPI, RT, BHE, SPIR + four saturation slabs	(1) RT, 4HB/83 (2) 3000/83	12 (4F, 8M)/31	50, 300, 700, 1000, 1300	(1) 0.59-0.63 (0.04-0.06) (2) 0.73-0.85 (0.25-0.36)
Chow *et al*[55], 2003	GE Signa	1.5	SS EPI	3000/(46.9-57.5)	12 (4F, 8M)/29	10, 300	1.047 (0.082)
Yoshikawa *et al*[57], 2006	Philips Intera	1.5	SS EPI, BH, SPIR	1500/66	185	0, 600	1.26 (0.23)
Bruegel *et al*[160], 2008	Siemens Avanto	1.5	SS EPI, NC, BH, FS	NR/69	96	50, 300, 600	0.82 (0.11)
Kiliçkesmez[64], 2008	Siemens Avanto	1.5	SS EPI, FB, FS	4900/93	50 (29F, 21M)/38.9	0, 500, 1000	1.28 (0.38)
Braithwaite *et al*[49], 2009	Siemens Trio	3.0	Stimulated Echo EPI, FB, FS	3200/76	20 (20M)/34.7	0, 400	1.28 (0.39)
[2]Saremi *et al*[161], 2011	a. SiemensAvanto b. SiemensTrio	a. 1.5 b. 3.0	SS SE EPI, FS (1) BH, no PI (2) BH, PI (3) FB, PI	(1) 150/75 (2) 144/72 (3) 174/87	13 (2F, 11M)/46 (13)	50, 400, 1000	a. 0.7 (0.05) b. 0.65 (0.08)
Miquel *et al*[34], 2012	Philips Achieva	1.5	SS SE EPI, FB	(5300-5800)/62	10 (7F, 3M)/32.3 (4.6)	100, 200, 500, 750, 1000	V1: 0.81 (0.06) V2: 0.82 (0.07)
Corona-Villalobos *et al*[58], 2013	Siemens Avanto	1.5	SS SE EPI, BH	(1) 3000/(69-79) (2) 2500/(76-95)	100 (36F, 64M)/60.4 (14.3)	(1) 0, 750 (2) 0, 50, 100, 200, 300, 450, 600, 750	(1) 0.90 (0.10) (2) 0.80 (0.08)
Klasen *et al*[63], 2013	Siemens Avanto	1.5	SS EPI	(6825-6930)/(68-76)	50 (30F, 20M)/55.1	50, 300, 600	O1: 0.774 (0.061) O2: 0.805 (0.081)
Donati *et al*[56], 2014	(1) Siemens Sonata (2) Siemens Trio (3) Philips Achieva (4) Philips Achieva (5) GE Signa (6) GE Discovery	1.5 3.0 1.5 3.0 1.5 3.0	SS SE EPI, FB, FS	(5000-6225)/(36-76)	10 (10M)/36.6 (7.7)	0, 1000	(1) 0.863 (0.092) (2) 0.775 (0.069) (3) 0.876 (0.153) (4) 0.851 (0.080) (5) 0.855 (0.138) (6) 0.888 (0.214)

Some studies were carried out with more *b*-values than specified in the following table to compute intravoxel incoherent motion-specific parameters. [1]Range for three diffusion directions; [2]Mean ADC of the three sequences reported in the paper. ADC: Apparent diffusion coefficient; F: Female; M: Male; NR: Not reported; SS: Single shot; MS: Multi-shot; SE: Spin echo; STEAM: Stimulated echo; EPI: Echo planar imaging; RF: Radiofrequency; RT: Respiratory triggered; NC: Navigator controlled; FB: Free breathing; BH: Breath-hold; BHI: Breath-hold end inspiratory; BHE: Breath-hold end expiratory; SPIR: Spectral pre-saturation with inversion recovery; V: Visit; O: Observer.

Table 4 Estimates of apparent diffusion coefficient values reported in human pancreatic body using a mono-exponential fit

Ref.	System	Field strength (T)	Sequence	TR/TE (ms/ms)	No. of Patients/mean age (SD) (year)	*b*-values (s/mm^2)	Mean ADC (SD) (× 10^{-3} mm^2/s)
Yamada *et al*[24], 1999	Siemens Vision	1.5	SS SE EPI, BH, FS	NR/123	78	0, 30, 300, 900, 1100	1.02 (0.28)
Chow *et al*[55], 2003	GE Signa	1.5	SS EPI	3000/(46.9-57.5)	12 (4F, 8M)/29	10, 300	2.605 (0.168)
Deng *et al*[156], 2006	Siemens Sonata	1.5	(1) SS SE EPI, BH	2000/82	9	0, 502	(1) 1.88 (0.27)
			(2) MS PROPELLER, FB, RT, FS + two saturation slabs	2000/105			(2) 2.14 (0.31)
Yoshikawa *et al*[57], 2006	Philips Intera	1.5	SS EPI, BH, SPIR	1500/66	124	0, 600	1.81 (0.41)
Kiliçkesmez *et al*[64], 2008	Siemens Avanto	1.5	SS EPI,FB, FS	4900/93	50 (29F, 21M)/38.9	0, 500, 1000	1.68 (0.26)
Braithwaite *et al*[49], 2009	Siemens	3.0	Stimulated Echo EPI, FB, FS	3200/76	20 (20M)/34.7	0, 400	2.63 (0.72)
Fattahi *et al*[65], 2009	Philips Intera	1.5	SS EPI, BH	1500/66	14 (11F, 3M)/46.1	0, 600	1.78 (0.07)
[1]Saremi *et al*[161], 2011	a. Siemens Avanto	a. 1.5	SS SE EPI, FS	(1) 150/75	13 (2F, 11M)/46 (13)	50, 400, 1000	a. 1.07 (0.1)
	b. Siemens Trio	b. 3.0	1. BH, no PI	(2) 144/72			b. 1.08 (0.1)
			2. BH, PI	(3) 174/87			
			3. FB, PI				
Thomas *et al*[167], 2012	Philips Achieva	1.5	SS EPI, FB, RT, FS	8000/90	38 (24F, 14M)/56	0, 800	1.77 (0.32)
Corona-Villalobos *et al*[58], 2013	Siemens Avanto	1.5	SS SE EPI, BH	(1) 3000/(69-79)	100 (36F, 64M)/60.4 (14.3)	(1) 0, 750	(1) 1.70 (0.22)
				(2) 2500/(76-95)		(2) 0, 50, 100, 200, 300, 450, 600, 750	(2) 1.26 (0.16)
Ma *et al*[168], 2014	GE Signa	3.0	SS SE EPI, BH, RT, FB, SPIR	(2275-5454)/58.8	21 (11F, 10M)/28.3 (3.6)	0, 500	BH: 1.57 (0.26)
							RT: 1.75 (0.28)
							FB: 1.71 (0.28)
Donati *et al*[56], 2014	(1) Siemens Sonata	1.5	SS SE EPI, FB, FS	(5000-6225)/(36-76)	10 (10M)/36.6 (7.7)	0, 1000	(1) 1.427 (0.165)
	(2) Siemens Trio	3.0					(2) 1.418 (0.189)
	(3) Philips Achieva	1.5					(3) 1.427 (0.212)
	(4) Philips Achieva	3.0					(4) 1.371 (0.193)
	(5) GE Signa	1.5					(5) 1.496 (0.220)
	(6) GE Discovery	3.0					(6) 1.621 (0.283)
Ma *et al*[153], 2015	GE Signa	3.0	SS EPI	6000/58.6	22 (13M)/63.7 (6.8)	0, 600	VOI: 1.44 (0.11)
							ROI: 1.40 (0.14)

Some studies were carried out with more *b*-values than specified in the following table to compute intravoxel incoherent motion-specific parameters. [1]Mean ADC of the three sequences reported in the paper. ADC: Apparent diffusion coefficient; F: Female; M: Male; NR: Not reported; SS: Single shot; MS: Multi-shot; SE: Spin echo; EPI: Echo planar imaging; RF: Radiofrequency; RT: Respiratory triggered; NC: Navigator controlled; FB: Free breathing; BH: Breath-hold; BHI: Breath-hold end inspiratory; BHE: Breath-hold end expiratory; SPIR: Spectral pre-saturation with inversion recovery; ROI: Single slice region of interest; VOI: Whole volume region of interest.

Prostate

Healthy prostate tissue ADC estimates of the central gland and peripheral zone from selected studies are presented in Table 6. Reported ADC values are higher in the peripheral zone (PZ) compared to the central gland (CG). The CG consists of more compact smooth muscle cells and sparser glandular elements than the PZ, leading to a lower extracellular-to-intracellular fluid ratio and to lower ADC values[74,75]. The highest reported ADC value in the PZ was 1.99 ± 0.208 × 10^{-3} mm^2/s[76] and the lowest was 1.25 ± 0.23 × 10^{-3} mm^2/s[77] leading to a median value of 1.64 × 10^{-3} mm^2/s. In the CG, the highest reported ADC value was 1.72 ± 0.35 × 10^{-3} mm^2/s[27] and the lowest was 0.9 ± 0.1 × 10^{-3} mm^2/s[78] leading to a median value of 1.31 × 10^{-3} mm^2/s. The majority of studies employed *b*-values of less than 800 s/mm^2. Average T_2-relaxation times of prostate are 88 ± 0 ms and 74 ± 9 ms at 1.5T and 3.0T respectively.

Potential usefulness of DW-MRI in localizing prostate cancer has been shown by a number of investigators[27,79,80]. DW-MRI is one of the criteria used in the scoring of the

Table 5 Estimates of apparent diffusion coefficient values reported in human gallbladder using a mono-exponential fit

Ref.	System	Field strength (T)	Sequence	TR/TE (ms/ms)	No. of patients/ mean age (SD) (yr)	*b*-values (s/mm^2)	Mean ADC (SD) (× 10^{-3} mm^2/s)
Yamada *et al*[24], 1999	Siemens Vision	1.5	SS SE EPI, BH, FS	NR/123	62	0, 30, 300, 900, 1100	2.81 (0.36)
Yoshikawa *et al*[57], 2006	Philips Intera	1.5	SS SE EPI, BH, SPIR	1500/66	151	0, 600	3.50 (0.51)
[1]Saremi *et al*[161], 2011	a. SiemensAvanto b. SiemensTrio	a. 1.5 b. 3.0	SS SE EPI, FS (1) BH, no PI (2) BH, PI (3) FB, PI	(1) 150/75 (2) 144/72 (3) 174/87	13 (2F, 11M)/46 (13)	50, 400, 1000	a. 2.6 (0.4) b. 2.6 (0.3)
Miquel *et al*[34], 2012	Philips Achieva	1.5	SS SE EPI, FB	(5300-5800)/62	10 (7F, 3M)/32.3 (4.6)	100, 200, 500, 750, 1000	V1: 2.93 (0.20) V2: 2.91 (0.21)
Corona-Villalobos *et al*[58], 2013	Siemens Avanto	1.5	SS SE EPI, BH	(1) 3000/(69-79) (2) 2500/(76-95)	100 (36F, 64M)/60.4 (14.3)	(1) 0, 750 (2) 0, 50, 100, 200, 300, 450, 600, 750	(1) 3.01 (0.33) (2) 2.74 (0.37)
Donati *et al*[56], 2014	(1) Siemens Sonata (2) Siemens Trio (3) Philips Achieva (4) Philips Achieva (5) GE Signa (6) GE Discovery	1.5 3.0 1.5 3.0 1.5 3.0	SS SE EPI, FB, FS	(5000-6225)/(36-76)	10 (10M)/36.6 (7.7)	0, 1000	(1) 2.585 (0.354) (2) 2.506 (0.223) (3) 2.657 (0.229) (4) 2.718 (0.327) (5) 2.670 (0.312) (6) 2.785 (0.477)

Some studies were carried out with more *b*-values than specified in the following table to compute intravoxel incoherent motion-specific parameters. [1]Mean ADC of the three sequences reported in the paper. ADC: Apparent diffusion coefficient; F: Female; M: Male; NR: Not reported; SS: Single shot; SE: Spin echo; EPI: Echo planar imaging; RF: Radiofrequency; RT: Respiratory triggered; NC: Navigator controlled; FB: Free breathing; BH: Breath-hold; BHI: Breath-hold end inspiratory; BHE: Breath-hold end expiratory; SPIR: Spectral pre-saturation with inversion recovery; PI: Parallel imaging.

likelihood of prostate cancer in the prostate imaging reporting and data system[81]. The majority of prostate cancer arises in the peripheral zone (68%)[82]. Although studies have demonstrated improved sensitivity and specificity in prostate cancer detection using DW-MRI, tumours smaller than 5 mm are difficult to detect[83]. Prostate transition zone is the site of benign prostatic hyperplastic nodules, which can have low ADC values and hence mimic tumour[83]. Post-biopsy haemorrhage in the prostate gland may cause susceptibility artefact[84] and add further uncertainty in the computed ADC map as it presents itself as a region of low signal intensity and hence mimic tumour[83]. Nevertheless, DW-MRI in combination with T_2-weighted imaging has been shown to be significantly better than T_2-weighted imaging alone in the detection of significant cancer within the peripheral zone of the prostate[80].

Gynaecologic sites

Gynaecologic DW-MRI comprises five main categories: Ovaries or fallopian tubes, endometrium, myometrium, cervix and vulva[85,86]. Gynaecologic healthy tissue ADC estimates are not often reported and only thirteen studies were included (Table 7) for normal endometrium (5), myometrium (3) and cervix (7). Range of reported ADCs for endometrium, myometrium and cervix in the selected publications are respectively (1.27 ± 0.22[87] - 1.53 ± 0.10[88]), (1.50 ± 0.20[87] - 1.62 ± 0.11[89]) and (1.41 ± 0.10[90] - 2.09 ± 0.46[91]) × 10^{-3} mm^2/s, leading to median values of 1.44, 1.53 and 1.71 × 10^{-3} mm^2/s respectively. Of the three anatomies, cervix has the greatest variation in ADC values, which could be attributed to its anatomical location. The air-tissue interface causes greater susceptibility-induced artefact in the acquired DW-MR images and the ADC estimate may vary considerably across studies due to the placement of the ROI. Average T_2-relaxation times for endometrium, myometrium and cervix are significantly different: 101 ± 21, 117 ± 14 and 58 ± 20 ms at 1.5T and 59 ± 1, 79 ± 10 and 83 ± 7 ms at 3.0T respectively[50]. DW-MRI can provide useful information in differentiating uterine endometrial cancer from benign lesions[88,92]. Tamai *et al*[88] demonstrated that there was no overlap between ADC values in normal endometrium and endometrial cancers. Nougaret *et al*[93] found a significant difference in the ADC values of grade 3 endometrial tumours compared to those of grade 1 and 2. However, in adjacent myometrium differentiating between benign and malignant disease based on ADC values alone is difficult[94]. In the ovaries, the majority of prior studies reported ADC values of benign and malignant lesions. Katayama *et al*[95] concluded that ADCs might not provide additional information in differentiating benign from malignant ovarian lesions, as there was a significant overlap[95-97] between ADCs in benign and malignant solid tumours. In the cervix, ADC values could play a role in the diagnosis[98] and as a surrogate biomarker of treatment response[99]. Luomaranta *et al*[100] concluded that DW-MRI is more reliable in the radiological staging of endometrial carcinoma compared with contrast-enhanced MRI.

Breast

Mammography is the modality of choice in breast scre-

Table 6 Estimates of apparent diffusion coefficient values reported in human prostate using a mono-exponential fit

Ref.	System	Field strength (T)	Sequence	TR/TE (ms/ms)	No. of patients/ mean age (SD)	*b*-values (s/ mm^2)	Mean ADC (SD) (× 10^{-3} mm^2/s)
[1]Gibbs *et al*[77], 2001	GE	1.5	SS SE EPI	4000/110	8/29	0, 720	CG: 1.17 (0.18) PZ: 1.25 (0.23)
Issa[169], 2002	GE	1.5	SS SE EPI	4000/120	7/29	64, 144, 257, 401, 578, 786	CG: 1.63 (0.30) PZ: 1.91 (0.46)
Sato *et al*[79], 2005	Siemens Symphony	1.5	SS SE EPI	2700/96	6	0, 300, 600	CG: 1.68 (0.26) PZ: 1.93 (0.24)
Pickles *et al*[170], 2006	GE Signa	3.0	SS SE EPI	4000/65.7	9/32	0, 500	CG: 1.27 (0.14) PZ: 1.60 (0.25)
Kumar *et al*[78], 2006	Siemens Avanto	1.5	SS SE EPI	3000/96	7/31.4 (3.6)	0, 250, 500, 750, 1000	CG: 0.9 (0.1) PZ: 1.5 (0.2)
Gibbs *et al*[171], 2007	GE Excite	3.0	SS SE EPI	4000/65.7	8/35	0, 500	CG: 1.21[2], 1.26[3] PZ: 1.56[2], 1.63[3]
Ren *et al*[172], 2008	Philips Intera	1.5	SS SE EPI	3000/63	16/37.9	0, 500	CG: 1.352 (0.052) PZ: 1.829 (0.071)
Kozlowski *et al*[76], 2008	GE Signa	1.5	(1) SS FSE (2) SS EPI	(1) 8000/87.5 (2) 8000/87.5	(1) 14 (2) 15	0, 600	(1) CG: 1.373 (0.179) PZ: 1.573 (0.270) (2) CG: 1.518 (0.126) PZ: 1.992 (0.208)
Tamada *et al*[173], 2008	GE Signa	1.5	SS SE EPI	5500/67.7	114/55 (1) 20 ≤ age ≤ 39 (*n* = 11) (2) 40 ≤ age ≤ 59 (*n* = 62) (3) 60 ≤ age ≤ 89 (*n* = 41)	0, 1000	(1) CG: 1.22 (0.10) PZ: 1.37 (0.18) (2) CG: 1.27 (0.12) PZ: 1.63 (0.26) (3) CG: 1.27 (0.12) PZ: 1.74 (0.25)
Riches *et al*[27], 2009	Philips Intera	1.5	SS SE EPI	2500/69	50/66 (6)	0, 800	CG: 1.72 (0.35) PZ: 1.66 (0.34)
Liu *et al*[174], 2013	GE Signa	3.0	SS SE EPI	4000/71.9	102	0, 1000	*n* = 69, CG: 1.36 (0.12) *n* = 74, PZ: 1.69 (0.28)
Emad-Eldin *et al*[74], 2014	Philips Intera	1.5	SS SE EPI	3600/110	12	0, 500, 800	CG: 1.469 (0.239) PZ: 1.839 (0.233)
[4]Peng *et al*[175], 2014	Philips Achieva	1.5	SS SE EPI, FB	(1) (2948-8191)/(71-79) (2) (3854-8616)/(83-85)	(1) 26/61.1 (7.2) (2) 25/62.0 (6.4)	(1) 0, 1000 (2) 0, 50, 200, 1500, 2000	PZ: (1) 1.75 (0.3) E (2) 1.33 (0.1) E

Some studies were carried out with more *b*-values than specified in the following table to compute intravoxel incoherent motion-specific parameters. [1]In this study 6 more *b*-values within the range were used; [2]Mean ADC over a short-term period of a few minutes between first scan and second scan; [3]Mean ADC over a medium-term of a month between first scan and second scan; [4]These authors reported the median values. ADC: Apparent diffusion coefficient; F: Female; M: Male; NR: Not reported; SS: Single shot; SE: Spin echo; EPI: Echo planar imaging; FSE: Fast spin echo; RF: Radiofrequency; RT: Respiratory triggered; NC: Navigator controlled; FB: Free breathing; BH: Breathhold; BHI: Breathhold end inspiratory; BHE: Breathhold end expiratory; SPIR: Spectral pre-saturation with inversion recovery; PZ: Peripheral zone; CG: Central gland; *n*: Number of patients; E: Estimate from the chart.

ening but is less effective in women with very dense breasts (higher content of fibroglandular tissue compared to fatty adipose tissue) and those with *BRCA1* genetic predisposition and MRI screening may offer added benefit[101-103]. Increasingly the added value of DW-MRI to the normal MRI screening particularly in dense breasts is being examined[104]. Normal fibroglandular breast tissue ADC estimates from selected studies are summarized in Table 8. The highest ADC estimate for normal fibroglandular breast tissue in selected studies was 2.37 ± 0.27 × 10^{-3} mm^2/s[105] and the lowest reported was 1.51 ± 0.29 × 10^{-3} mm^2/s[182] leading to a median value of 1.92 × 10^{-3} mm^2/s. The majority of DW-MR studies in the breast investigated lesion detection and characterisation[105-107]. Some focused on the measured ADC values during different weeks of the menstrual cycle[17,108] while others focused on the significance of pre- and post-menopausal ADC values[109]. Average T_2-relaxation times of breast fibroglandular tissue and that of fatty adipose tissue at 1.5T field strength were reported as 40 ± 10 ms and 130 ± 10 ms/380 ± 30 ms (two values corresponding to the dominant lipid peaks) respectively[110]. This relatively short T_2-relaxation time of normal fibroglandular breast tissue must be considered when optimizing *b*-values for DW-MRI studies.

Suppression of lipid signal in DW-MRI of the breast is essential to reduce image artefacts and to increase lesion detection[111]. Different fat suppression techniques were compared in few studies[112-114] whereby significant differences in the computed ADC values were observed between spectral fat suppression (SPAIR) and short-time inversion recovery (STIR) techniques[112] and a larger overlap in ADC values between tumour and benign tissue was detected using STIR[112]. However, the authors in[113]

Table 7 Estimates of apparent diffusion coefficient values reported in human Uterus (endometrium, myometrium and cervix) using a mono-exponential fit

Ref.	System	Field strength (T)	Sequence	TR/TE (ms/ms)	No. of patients/ mean age (SD)	*b*-values (s/mm^2)	Mean ADC (SD) ($\times 10^{-3}$ mm^2/s)
Naganawa *et al*[99], 2005	Siemens Symphony	1.5	SS SE EPI	2500/96	10/46.6	0, 300, 600	Cervix, 1.79 (0.24)
Tamai *et al*[88], 2007	Siemens Symphony	1.5	SS SE EPI, FS	4400/(74-99)	12/49	0, 500, 100	Endometrium, 1.53 (0.10)
Zhang *et al*[176], 2007	Philips Intera	1.5	SS SE EPI	6800/70	(9 + 7V)/34 median	0, 800	Cervix, 1.71 (0.14)
McVeigh *et al*[91], 2008	GE Signa	1.5	SS SE EPI	4000/68	30/47	0, 600	Cervix *n* = 26, 2.09 (0.46)
Shen *et al*[92], 2008	GE Excite	1.5	SS SE EPI	8000/83	7/45.2	0, 500, 800, 1000	Endometrium, 1.277 (0.219)
Fujii *et al*[177], 2008	Siemens Symphony	1.5	SS SE EPI, STIR FS, FB	(9500-9800)/(73-78)	26/53	0, 1000	Endometrium *n* = 25, 1.44 (0.34)
Tamai *et al*[89], 2008	Siemens Symphony	1.5	SS SE EPI, FS	(2700-4400)/(78-90)	43/48	0, 500, 1000	Myometrium, 1.62 (0.11)
Inada *et al*[178], 2009	GE Signa	1.5	SS SE EPI, FB	(3400-7500)/68	31/44.9 (12.7)	0, 800	Endometrium, 1.52 (0.20) Myometrium, 1.53 (0.25)
Liu *et al*[179], 2009	GE Excite	1.5	SS EPI	4000/58.5	57	0, 1000	Cervix, 1.50 (0.16)
Payne *et al*[180], 2010	Philips Intera	1.5	SS SE EPI	4500/80	62/38	0, 100, 300, 500, 800	Cervix *n* = 43, 1.769 (0.239)
Chen *et al*[98], 2010	Philips Intera	1.5	SS SE EPI, STIR FS	6800/70	20/34.4	0, 800	Cervix, 1.593 (0.151)
Cao *et al*[87], 2012	GE Signa	1.5	SS SE EPI, FB	NR/NR	64/55.4	0, 1000	Endometrium, 1.267 (0.221) Myometrium, 1.496 (0.196) Junctional zone, 1.126 (0.190)
Kuang *et al*[90], 2013	Siemens Trio	3.0	SS SE EPI, FS	AX: 7000/71, SAG: 1800/76	67	(1) 0, 600 (2) 0, 1000	Cervix, (1) 1.55 (0.28) (2) 1.41 (0.10)

Some studies were carried out with more *b*-values than specified in the following table to compute intravoxel incoherent motion-specific parameters. ADC: Apparent diffusion coefficient; NR: Not reported; SS: Single shot; SE: Spin echo; EPI: Echo planar imaging; RF: Radiofrequency; RT: Respiratory triggered; NC: Navigator controlled; FB: Free breathing; BH: Breath-hold; BHI: Breath-hold end inspiratory; BHE: Breath-hold end expiratory; *n*: Number of patients; STIR: Short TI inversion recovery; FS: Fat suppression; NA: Not available; AX: Axial; SAG: Sagittal; W: Week; V: Volunteer.

found that the computed ADC values using SPAIR and STIR fat suppression techniques were very similar. In another study[114] four types of STIR, SPAIR, spectrally adiabatic inversion recovery and water excitation were compared of which water excitation yielded the highest signal-to-noise. Regardless of the choice of the fat suppression technique, multi-centre studies are required to standardise DW-MRI parameters and to establish the clinical utility of DW-MRI and ADC values of malignant and benign disease[111].

Cancer vs normal tissue

DW MRI is already being incorporated into general oncologic imaging practice. One of its main advantageous is that it does not require intravenous contrast media enabling its use in patients with reduced renal function[5]. Increase in tumour cellularity and architectural distortion contribute to decreased ADC values. In tissues that are highly cellular, tortuosity of the extracellular space and the higher density of hydrophobic cellular membranes restrict the apparent diffusion of water protons[23,115,116]. Therefore it is expected that ADC values would correlate with tumour cellularity and grade as it has been shown in[117]. In Table 9 reported ADC values of malignant *vs* normal tissue from selected studies in different anatomical regions are shown. In the majority of oncologic studies, a significant change in ADC has been detected between each of the malignant disease, benign and normal tissue. Radiologists use increased tumour cellularity as a biomarker of malignancy using DW-MRI to differentiate between benign and malignant disease[47,28,118]. However, tumour necrosis and nuclear atypia can account for imperfect correlations between ADC values and cellularity with necrosis being an intrinsic component of poorly differentiated tumours as it increases ADC values[16]. Other clinical oncologic uses include monitoring treatment response after chemotherapy or radiation, differentiating post-therapeutic changes from residual active tumour and detecting recurrent cancer[5]. Potential future applications include predicting treatment outcomes before and after therapy, tumour staging and detecting lymph node involvement by cancer[5]. There is much contention about these potential applications of DW-MRI and its potential role in differentiating between tumour grades. Unsubstantiated claims have been made in the literature about tumour staging. The authors in[119] staged breast tumour grades based on statistically insignificant changes in the median ADC (grade 1 ADC 1.11 mm^2/s, grade 2 ADC 1.10 mm^2/s and grade 3 ADC 1.06 mm^2/s). This is in contrast to the study conducted in[117] where there was a statistically significant change in the mean ADC between a high-grade glioma (ADC 1.2 mm^2/s) and a low-grade glioma (ADC 2.7 mm^2/s). The authors in[120] also differentiated between endometrial tumour

Table 8 Estimates of apparent diffusion coefficient values reported in the normal fibroglandular breast tissue using a mono-exponential fit

Ref.	System	Field strength (T)	Sequence	TR/TE (ms/ms)	No. of patients/ mean age (SD)	*b*-values (s/mm^2)	Mean ADC (SD) (× 10^{-3} mm^2/s)
Englander *et al*[181], 1997	GE Signa	1.5	SE	(2 or 3)HB/100	4/32 (2.6)	12.48, 611.31, 199.61, 449.12, 77.97, 311.89, 112.28	1.64 (0.19)
Partridge *et al*[17], 2001	GE Signa	1.5	SS FSE	8000/86	8/27	0, 578	*n* = 6, W1: 1.72 (0.23) W2: 1.61 (0.22) W3: 1.66 (0.17) W4: 1.75 (0.17)
Sinha *et al*[105], 2002	GE Signa	1.5	SS EPI	5000/72	16	0, 269, 537, 806, 1074	2.37 (0.27)
Woodhams*et al*[106], 2005	GE Signa	1.5	SS SE EPI	5000/61.8	190/53	0, 750, 1000	2.09 (0.27)
Park *et al*[182], 2007	GE Signa	1.5	SS EPI	6000/75	41/53.1	0, 1000	1.51 (0.29)
Yoshikawa *et al*[107], 2008	Philips Intera	1.5	SS SE EPI	6238/90	27	0, 200, 400, 600, 800	1.96 (0.21)
Kim *et al*[119], 2009	GE Signa	1.5	SS SE EPI	6000/75	67/54	0, 1000	1.59 (0.27)
Baron *et al*[114], 2010	Siemens Avanto	1.5	SS SE EPI, (1) FS (2) STIR (3) SPAIR (4) WaterExcitation	3000/93	7/26.6	0, 20, 40, 60, 80, 100, 150, 200, 300, 400, 500, 600	(1) 1.99 (2) 2.02 (3) 2.03 (4) 2.06 overall 2.03 (0.03)
Partridge *et al*[44], 2010	GE Signa	1.5	SS SE EPI	7 s/71.5	12/36 (median)	0, 600, 1000	1.95 (0.24)
O'Flynn *et al*[109], 2012	Philips Achieva	3.0	SS SE EPI, SPAIR, SSGR	3771/67	31/45.9 13 PRM/36.6 18 PM/55.2	(1) 0, 100, 150, 200, 350, 700, 1200 (2) 100, 150, 200, 350, 700, 1200	PRM, (1) 1.84 (0.26) (2) 1.77 (0.26) PM, (1) 1.46 (0.3) (2) 1.33 (0.3)
Tagliafico *et al*[183], 2012	GE Signa	3.0	SS EPI	16675/NR	60/57 (median)	0, 1000	1.92 (0.30)
AlRashidi *et al*[108], 2012	Philips Achieva	3.0	SS SE EPI, SPAIR	9543/50	26	0, 50, 150, 800	MC, W1: 2.18 (0.38) W2: 2.20 (0.39) W3: 2.22 (0.38) W4: 2.22 (0.33)
McDonald *et al*[184], 2014	Philips Achieva	3.0	SS SE EPI	5336/61	103/47 (11)	0, 800	1.62 (0.30)

Some studies were carried out with more *b*-values than specified in the following table to compute intravoxel incoherent motion-specific parameters. ADC: Apparent diffusion coefficient; F: Female; M: Male; NR: Not reported; SS: Single shot; SE: Spin echo; EPI: Echo planar imaging; FSE: Fast spin echo; RF: Radiofrequency; RT: Respiratory triggered; NC: Navigator controlled; FB: Free breathing; BH: Breath-hold; HB: Heart beats; n: Number of patients; SPAIR: Spectral selection attenuated inversion recovery; SSGR: Slice selection gradient reversal; FS: Fat suppression; AX: Axial; SAG: Sagittal; MC: Menstrual cycle; PM: Post-menopause; PRM: Pre-menopause; W: Week; L: Left; R: Right.

grades based on statistically insignificant changes in the mean ADCs, however, they were confidently able to differentiate between benign and malignant disease. The utility of ADC was also investigated in ultrasound-guided biopsies in the detection and localization of prostate cancer. In a large-scale cohort study of 1448 patients[121] who underwent systematic biopsies (890 patients with low-ADC lesions underwent additional targeted biopsies), the authors demonstrated that targeted biopsy strategy based on ADC maps can be useful in the patient selection for subsequent prostate biopsies and in the detection and localization of prostate cancer to high accuracy.

REPRODUCIBILITY OF ADC VALUES

In this section a literature survey of the repeatability and reproducibility of ADC values both in phantoms and *in vivo* is provided. Repeatability refers to test conditions that are as constant as possible, where the same operator using the same equipment within a "short time interval" obtains independent test results with the same method on identical items in the same laboratory[122]. On the other hand, "reproducibility refers to test conditions under which results are obtained with the same method on identical test items but in different laboratories with different operators using equipment"[122]. Therefore repeatability informs on equipment variation while reproducibility informs on observer/experimental variation[5].

Bland-Altman plots[123] are frequently used to show any trends in the variability of ADC measurements over the measuring interval. Bland-Altman plots help to illustrate the bias-variance relationship and limits of agreement[124]. The basis for estimates of repeatability

Table 9 Estimates of apparent diffusion coefficient values of cancer *vs* normal tissue/benign disease reported in selected studies on different anatomical regions using a mono-exponential fit

Ref.	Anatomical region	Journal	Tumour and tissue	No. of subjects	*b*-values (s/mm^2)	Mean ADC (SD) (× 10^{-3} mm^2/s)
Kim *et al*[29], 1999	Liver	*AJR*	Malignant	49	3, 57, 192, 408, 517,	1.01 (0.38)
			Normal liver	48	705, 846	1.92 (0.32)
[1]Taouli *et al*[47], 2003	Liver	*Radiology*	Metastatic lesions	15	(1) 0, 500	(1) Lesions 0.94 (0.60)
			Normal liver	14	(2) 0, 134, 267, 400	Normal 1.83 (0.36)
						(2) Lesions 0.85 (0.51)
						Normal 1.51 (0.49)
Sato *et al*[79], 2005	Prostate	*JMRI*	Prostate cancer	23	0, 300, 600	1.11 (0.41)
			Normal prostate	23		1.68 (0.40)
Naganawa *et al*[99], 2005	Cervix	*European Radiology*	Cervical cancer	12	0, 300, 600	1.09 (0.20)
			Normal cervix	10		1.79 (0.24)
McVeigh *et al*[91], 2008	Cervix	*European Radiology*	Cervical cancer	47	0, 600	1.09 (0.20)
			Normal cervix	26		2.09 (0.46)
Yoshikawa *et al*[107], 2008	Breast	*Radiation Medicine*	IDC	24	0, 200, 400, 600,	1.07 (0.19)
			NIDC	3	800	1.42(0.17)
			Normal breast	27		1.96(0.21)
Kim *et al*[119], 2009	Breast	*JMRI*	Breast cancer	62	0, 1000	1.09 (0.27)
			Normal breast	67		1.59 (0.27)
Riches *et al*[27], 2009	Prostate	*NMR in Biomedicine*	Prostate cancer	43	0, 800	1.33 (0.52)
			Central gland	50		1.72 (0.35)
			Peripheral zone	50		1.66 (0.34)
Fattahi *et al*[65], 2009	Pancreas	*JMRI*	Pancreatic cancer	10	0, 600	1.46 (0.18)
			Normal pancreas	14		1.78 (0.07)
Sugita *et al*[185], 2009	Gallbladder	*European Radiology*	Gallbladder carcinoma	15	0, 1000	1.28 (0.41)
			Gallbladder disease	14		1.92 (0.21)
Taouli *et al*[186], 2009	Kidney	*Radiology*	RCC	64 (28 RCC)	0, 400, 800	1.41 (0.61)
			Benign lesions	64 (81 benign lesions)		2.23 (0.87)
Wang *et al*[187], 2010	Kidney	*Radiology*	RCC	83	(1) 0, 500	(1) RCC 1.849 (0.399)
			RP		(2) 0, 800	RP 2.455 (0.238)
						(2) RCC 1.698 (0.323)
						RP 2.303 (0.172)
Cao *et al*[87], 2012	Uterus	*European Journal of Radiology*	Endometrial carcinoma	13	0, 1000	1.011 (0.102)
			Normal endometrium	64		1.267 (0.221)
Ogawa *et al*[188], 2012	Gallbladder	*Journal of Gastroenterology*	Gallbladder carcinoma	36	0, 1000	1.83 (0.69)
			Gallbladder disease	117		2.60 (0.54)

Some studies were carried out with more *b*-values than specified in the following table to compute intravoxel incoherent motion-specific parameters. [1]Authors in this study used two different DW sequences. IDC: Invasive ductal carcinoma; NIDC: Noninvasive ductal carcinoma; RCC: Renal carcinoma; RP: Renal parenchyma; DW: Diffusion-weighted.

is the within-subject variance assuming that all other factors have been controlled through experimental design[124]. Within-subject variance may include biological or physiological variability as well as patient repositioning and scanner calibrations[124]. Repeated-measures analysis of variance (rm-ANOVA) is used to assess differences in ADC values measured at each *b*-value between magnetic field strengths[125]. Inter-reader agreement regarding ADC measurements is frequently assessed by computing the intra-class correlation coefficient (ICC)[5,56]. ICC is a measure of repeated measures consistency relative to the total variability in the population[124]. The within-subject coefficient of variation is often reported for repeatability studies to assess repeatability in test-retest designs[124]. One-way analysis of variance (one-way ANOVA) is usually used to test discrepancy between the highest and lowest values and difference in these results among MR scanners[126]. Bonferroni correction is typically used to counteract the problem of multiple testing[56,125]. Statistical significance is usually assessed at $P < 0.05$[125,126].

"A good qualified biomarker should have three properties: Biological relevance to the disease process under study, sensitivity to the disease process and good reproducibility"[127]. In clinical trials questions revolve around whether changes in individual patients can be measured reliably and reproducibly and whether they predict important clinical outcomes in terms of monitoring response to therapy[5,128]. Reproducibility measurements of DW-MRI data are necessary to understand the magnitude of variation that can be detected confidently. Both the size and the position of lesions are known to influence reproducibility, with larger lesions being more reproducible[129]. At the time of authoring

this review, 1860 Google Scholar entries were found for (ADC + MRI + repeatability) and 8200 for (ADC + MRI + reproducibility). However, the mere use of the word repeatability and reproducibility in the entries, does not indicate an elaborate study into repeatability and reproducibility of ADC values. In a serial single-centre study, to establish treatment effect, each subject will normally be scanned at the same centre at each time point and it is the within-subject variance measured at a given centre, over the duration of the study, which is important. If the study is to be multi-centre "then between-centre variance should also be controlled"[127]. The within-centre variance for a subject or repeatability is important and it is measured using the Bland-Altman analysis method[123]. In single centre studies, "repeated measurements are usually made in pairs over a set of subjects (typically 5-20) to establish the difference between repeats and whether this depends on the mean value of the parameter being estimated"[127]. In multi-centre studies, protocol matching is the simplest method of reducing measurement differences[127] although "differences in imaging hardware produced by different vendors may prevent identical protocols being used at every site".

ADC maps are quantitative imaging maps, which in principle are "independent of the particular imaging protocols used"[127] although in reality significant variations in ADC values of different anatomical regions have been reported both in single-centre and in multi-centre studies[126].

In the following discussions the words (Philips, Siemens, GE and Toshiba) refer to MR system vendors Philips (Philips Healthcare, Best, The Netherlands), Siemens (Siemens Healthcare, Erlangen, Germany), GE (GE Healthcare, Waukesha, WI) and Toshiba (Toshiba Medical Systems, Tokyo, Japan).

Reproducibility of ADC values in vitro

Phantoms have three advantages over human control subjects. First, phantoms can be scanned repeatedly "without any ethical constraints", second, they have "known physical properties" and third, they are "relatively easy to transport between centres"[127]. Potential disadvantages include "a lack of realism compared to *in vivo* measurements", "MR properties of the material progressively vary with time" and "the time and expertise required to build phantoms are prohibitive at some centres"[127]. Some phantoms have been developed to measure some tissue properties that exist in tumours[130]. Phantom measurements have been made with alkanes[131] or other organic liquids[132], which have ADC values in the range of brain tissue. Other materials include sucrose solutions[133,134], iced water[125] and gels[135,136].

Chenevert *et al*[125] (2011) proposed a novel ice-water phantom for DW-MRI multi-centre trials and investigated ADC variability across 20 MR scanners from 3 vendors (GE, Philips, Siemens) at 7 institutions at both 1.5T and 3.0T field strengths. To assess single-system repeatability, the phantom was also imaged on 16 different days over a period of 25 d. Site-specific DW-MRI protocols were performed as well as a standard DW-MRI protocol with *b*-values of 0, 500, 800, 1000, 2000 s/mm^2. Vendor-independent software was used to compute the ADC maps. Magnet field strength was not found to have an impact on ADC measurements, however, significant differences in ADC measurements were observed between vendors. The authors reported a ± 5% variation in ADC across all systems and single-system repeatability was also ± 5%. Malyarenko *et al*[137] (2013) reported a multi-centre study using a variation of the ice-water phantom developed by Chenevert *et al*[125]. The authors devised a DW-MRI protocol compatible across 35 clinical MRI platforms (GE, Philips, Siemens) at 18 institutions at two field strengths of 1.5T and 3.0T. Vendor-independent software was used to compute the ADC maps. Standard deviation of ADCs measured at the magnet's isocentre was less than 2% for all 35 platforms. Inter-site reproducibility of ADC at magnet isocentre was within 3%. ADC variability increased for off-centre measurement consistent with diffusion gradient non-linearity. Overall the authors concluded that standardization of DW-MRI protocol improved reproducibility of ADC measurements and allowed identification of non-linearity in the diffusion gradients as a source of error in the measured ADC in clinical multi-centre trials. Kıvrak *et al*[138] (2013) used an in-house phantom consisting of four containers filled with distilled water, 0.9% NaCl, 25% NaCl and shampoo placed into a plastic container containing tap water. DW-MRI imaging of the phantom was performed using six different scanners from four vendors (Toshiba, GE, Philips and Siemens) utilizing a multichannel head coil and *b*-values of 0 and 1000 s/mm^2 at a room temperature of 21℃. ADC maps were computed on seven vendor-specific workstations. Statistically significant variations in ADC values for each fluid of the phantom were recorded between some scanners. Intra-vendor variability in ADC values was statistically significant for some scanners but not others. Overall the authors concluded that there were significant intra-vendor and inter-vendor variations in the computed ADC values. Giannelli *et al*[139] (2014) used an in-house isotropic water (per 1000 g distilled water: 1.25 g $NiSO_4.6H_2O$ + 5 g NaCl) phantom made of two cylindrical bottles to resemble female breast. DW-MRI of the phantom was performed using three scanners from three vendors (Philips, Siemens, GE) at 1.5T field strength. Two *b*-values of 0 and 850 s/mm^2 were used to sensitize diffusion and a total of 5 acquisitions were repeated for each scanner. Vendor-independent software was used to compute the ADC maps. ADC values were found to be significantly different between scanners. Coefficient of variation for repeated measurements was less than 1% while it had a mean value of 6.8% across scanners. Overall the authors concluded that a specific quality control protocol must be devised for DW-MRI of the human breast as system-induced variations were found to be substantial.

Belli *et al*[140] (2015) reported extensive assessment of ADC variability on 35 MR scanners (1.0T: 2.7%, 1.5T: 65.7% and 3.0T: 31.6%) from 26 participating centres. Standard doped water phantoms were developed at the coordinating centre using cylindrical bottles filled with an aqueous solution of 2 mmol/L of hexahydrate $NiCl_2$ and 0.5 g/L NaN_3. Two DW-MRI sequences were used in this study: First sequence with *b*-values ranging from 0 to 1000 s/mm^2 in steps of 100 s/mm^2 and second sequence with *b*-values ranging from 0 to 3000 s/mm^2 in steps of 500 s/mm^2. No parallel imaging technique was employed and vendor-independent software was used to generate the ADC maps. ADCs were normalized to 20 ℃ to assess inter-scanner variability. No statistical significance was detected for the ADCs estimated from the first DW sequence between 1.5T and 3.0T scanners while ADC estimates of the second DW sequence were significantly different between the two field strengths. Overall ADC measurements were within 5% from the nominal value and the highest deviation and overall standard deviation were 9.3% and 3.5% respectively. The authors carried out a second set of measurements on 26 scanners whereby short-term repeatability was assessed by repeating the first DW sequence five times at 1-min intervals. Short-term repeatability of ADC measurement was found to be less than 2.5% for 26 MR scanners. Doblas *et al*[141] (2015) reported a 7 centre multi-vendor study in which the reproducibility of ADC values was assessed on preclinical systems at field strengths of 4.7T, 7.0T and 9.4T. A miniaturized ice-water phantom was designed which was adapted from a previously reported clinical design[125]. Site-specific post-processing software packages were used to compute the ADC maps in which *b*-values less than 100 s/mm^2 were excluded from the computation. Inter-site ADC reproducibility was 6.3% and no site was identified as presenting different measurements than others. Mean day-to-day repeatability of ADC measurements was 2.3%. Between-slice ADC variability was insignificant and mean within ROI ADC variability was 5.5%. Overall the authors concluded that with the use of standardized protocols, ADC values are comparable between sites and vendors.

Reproducibility of ADC values in vivo

In MRI studies, human control subjects have three advantages over phantoms. First they can be an almost complete simulation of the clinical measurement process in a multi-centre study, second demands for temperature stabilization are bypassed as homeostasis provides inbuilt temperature control and third human controls are often more readily available than phantoms[127]. Disadvantages include a lack of measurement stability over time for tumour-related parameters in patients, imaging humans is more demanding of resources compared to imaging phantoms and ethical constraints may limit the availability of human subjects[127]. Despite these limitations, a number of DW-MRI studies have reported ADC measurement repeatability and reproducibility using human subjects. Sasaki *et al*[126] (2008) studied variability of ADC values of grey and white matter in 12 healthy volunteers, within a time frame of 2 wk, using 10 systems from four different vendors (Philips, Siemens, GE, Toshiba) at 1.5T and 3.0T field strengths and *b*-values of 0 and 1000 s/mm^2. Three different coils (multichannel coil with sensitivity correction, multichannel coil without sensitivity correction and a quadrature detection coil) were used to acquire the images and vendor-independent software was used to compute the ADC maps using a mono-exponential fit. The ADC values for gray and/or white matter of the same volunteers varied significantly between systems of all the vendors with an inter-vendor variability as high as 7%. There was also significant intra-system variability of up to 8% depending on the coil configuration in certain systems. Overall the authors concluded that there was significant variability in the ADC values. Braithwaite *et al*[49] (2009) tested the hypothesis that, "there is no significant variability in ADCs in the assessment of short- and midterm reproducibility of ADC measurements in a healthy population", in five abdominal locations on a population of 20 healthy male volunteers at 3.0T using *b*-values of 0 and 400 s/mm^2. All 20 volunteers were scanned once on the same day using 5 repeated DW-MRI acquisitions in the abdomen and 16 of the volunteers underwent a second scan within a time frame of 147 ± 20 d using another set of 5 repeated DW-MRI acquisitions. Vendor-specific software was used to generate the ADC maps and 3 ROIs were drawn for each anatomical location. Highly significant differences in the mean ADCs between the five anatomical locations were observed. No significant differences in the ADCs among the various sequence repetitions were observed. Between the two imaging sessions, no significant differences in mean ADC values were observed. Overall, the mean CV for the reproducibility of ADCs over short- and midterm was 14% and based on their results the authors suggested that ADCs are robust and can serve as a reliable quantitative tool over time. However, they also concluded that treatment effects of less than approximately 27% would not be clinically detectable with confidence with one acquisition in a single individual. Colagrande *et al*[142] (2010) compared ADC measurement repeatability and reproducibility of a phantom to that of abdominal DW-MRI on 30 healthy volunteers at 1.5T field strength. For the phantom study two DW-MRI sequences were employed: *b*-values ranging 0-200 s/mm^2 (steps of 20 s/mm^2) and *b*-values ranging from 0-1000 s/mm^2 (steps of 100 s/mm^2). For the volunteer study, *b*-values of 0 and 1000 s/mm^2 were used. Vendor-independent software was used to compute the ADC maps. Overall the authors concluded that the ADC values were repeatable with an ICC of 0.80 but not reproducible (ICCs ≤ 0.45) for all methods. Larger ROIs improved reproducibility and the authors advised that for larger studies standardized ADC measurements using more than two observers are needed. Miquel *et al*[34] (2012) compared repeatability of the ADC measure-

ments of a phantom containing copper sulphate ($CuSO_4$ 3 mmol/L) and salt (NaCl 34 mmol/L) solution with that of the abdomen on 10 healthy volunteers at 1.5T field strength using six *b*-values ranging from 0 to 1000 s/mm^2 (with the exception of zero, all *b*-values were greater than 100 s/mm^2). The phantom was imaged 10 times on two different occasions and also at regular intervals over a period of three months at a room temperature of 17 ℃ ± 0.5 ℃. A circular ROI covering 90% of the cross-section of the phantom bottle was selected on each slice. On the first day the CV of the ADC was 0.5% for 10 measurements and on day 100 the CV was 1.0% for 10 measurements. The mean intra-slice CV was 3.2% ± 1.4% and the mean sample CV was 2.9% ± 1.0%. Repeatability of the volunteer population was assessed on two occasions, 5.8 ± 1.9 d apart. The authors carried out two sets of analyses: One on volumes-of-interest (VOIs) and one on multiple smaller ROIs. Both intra-observer and inter-observer variability were small. Collectively there was no statistical difference in the group mean ADC value between the two visits of any organ. The authors concluded that larger three-dimensional VOIs result in lower variability compared to multiple two-dimensional ROIs, which depending on organs changes of over 7%-10% being significant, increasing to 20%-28% for ROIs. Bilgili[143] (2012) studied repeatability of the ADC measurements of the abdomen on 11 healthy volunteers during two repeat sessions at 1.5T field strength and using *b*-values of 0 and 500 s/mm^2. No significant differences in the ADCs for any organ between imaging sessions were found. The CV values ranged between 7.3% for the liver and 10.4% for the kidney at a *b*-value of 500 s/mm^2. Barral (2013) *et al*[68] evaluated variations in ADC measurements in normal pancreatic parenchyma at 1.5T and 3.0T field strengths using Siemens scanners. Two populations of twenty patients, who were matched for gender and age, were examined using a range of *b*-values from 0-800 s/mm^2 (6 *b*-values were less than 100 s/mm^2) with the first population examined at 1.5T and the second at 3.0T. Vendor software was used to compute the ADC maps using 3 *b*-values of 0, 400 and 800 s/mm^2. Four pancreatic segments namely head, neck, body and tail were evaluated in this study by two independent observers. ADCs were measured three times by each observer. No significant differences in ADCs were found between repeated measurements and between ADCs obtained at both field strengths. The 95% limits of agreements between ADC values ranged from 1%-24.2% for intra-observer and from 4.2%-25% for inter-observer variability and did not vary substantially at either field strengths. No significant differences in ADCs of the four segments were found at either field strength. Donati *et al*[56] (2014) performed DW- MRI on 10 healthy men to determine the variability of ADC values in various anatomical regions in the upper abdomen using six systems from three different vendors (Philips, Siemens, GE) at 1.5T and 3.0T field strengths. In this study, 10 *b*-values ranging from 0 to 1000 s/mm^2 (five *b*-values were less than 100 s/mm^2) were used and vendor-independent software on an independent workstation was used to compute the ADC maps. Two readers examined the images and they found that the inter-reader agreement was excellent with an intra-class correlation coefficient of 0.876. Overall, the highest coefficient of variations (CV) was observed in the liver for both field strengths and the lowest CVs were observed in the kidney. CVs ranged from 7.0% for renal medulla to 27.1% for left liver lobe. No significant differences in mean ADC values measured at 1.5T or 3.0 T were found in any of the evaluated anatomical regions. However, they concluded that the particular vendor of an MR system influences the ADC values to a lesser extent at 1.5T than 3.0T. Chen *et al*[144] (2014) compared ADC variability in normal liver parenchyma obtained with multiple breath-hold, free-breathing, respiratory-triggered and navigator-triggered DW-MRI techniques at 1.5T field strength using *b*-values of 0, 100 and 500 s/mm^2. The authors placed ROIs on 9 anatomical liver locations and did not observe any significant difference between ADCs obtained using different techniques. However, they concluded that both anatomical location and DW-MRI technique influence the reproducibility of liver ADC measurements. Jajamovich *et al*[145] (2014) investigated short-term reproducibility of the measured ADC in fasting conditions and after a liquid meal. Thirty individuals (11 healthy volunteers and 19 liver disease patients) were scanned twice after 6 h of fasting (5 min interval between scans) and then a third time 20 min after a liquid meal using a GE scanner at 3.0T field strength. Sixteen *b*-values were used in this study with 7 *b*-values < 100 s/mm^2 and 9 *b*-values ≤ 800 s/mm^2. Vendor-independent software was used to compute the ADC maps using both a mono-exponential model (*b*-values of 0 and 800 s/mm^2) and a bi-exponential model (all *b*-values). Coefficient of variation in the fasting condition was found to be 8.2% and 15.2% for the mono-exponential model and the bi-exponential model respectively. No effect was observed in the measured ADC following caloric intake, however, a substantial effect was observed in the hepatic portal vein flow. Pazahr *et al*[146] (2014) assessed changes in the measured ADC of the liver before and after carbohydrate and protein-rich food intake in correlation to hepatic portal vein flow quantified using phase contrast imaging. Ten healthy volunteers underwent 4 DW-MRI scans using a 1.5T field strength GE scanner on two days. Scans 1 and 2 on the same day one with at least 8 h of fasting and the second 30 min after intake of a protein-rich drink. On the second date volunteers were first scanned after fasting for 8 h and then after intake of a carbohydrate-rich meal. Diffusion *b*-values of 0, 50, 150, 250, 500, 750 and 1000 s/mm^2 were used in this study. Vendor-independent software was used to compute the ADC maps using a tri-exponential diffusion model with a linear fit to logarithmic signal intensities at *b*-values of 0 and 50 s/mm^2, 50 to 250 s/mm^2 and 500 to 1000 s/mm^2. A phantom filled with an aqueous solution of 770 mg/L

of $CuSO_4.5H_2O$ was used to assess the DW-MRI sequence and the post-processing software. ROIs were drawn on the right hepatic lobe. No significant statistical differences were found between measured ADC values after fasting and after protein-rich meal or carbohydrate-rich meal for the three sets of low, intermediate and high *b*-values. Overall mean CVs for each participant at each session were 13.9%, 7.2% and 7.5% for low, intermediate and high *b*-values respectively. The authors concluded that carbohydrate and protein-rich intake both resulted in a significant increase in the portal vein flow and that there was no correlation between the increase in the portal vein flow and the measured ADC values. They also recommended that liver molecular water diffusion should be quantified using *b*-values greater than 500 s/mm^2 only. Kolff-Gart *et al*[147] (2015) investigated variability of ADC values in the head and neck tissues on 7 healthy volunteers in 2 institutions using 5 MRI systems from three vendors (Philips, Siemens, GE) at 3 time points. They used two DW-MRI sequences: An EPI and a TSE using 2 *b*-values of 0 and 1000 s/mm^2 and an additional 6 *b*-value (two of the *b*-values were less than 100 s/mm^2) acquisition for the EPI sequence. Vendor-specific software was used to compute the ADC maps. Inter-system difference for mean ADC values and the influence of the MRI system on ADC values among the subjects were statistically significant. Mean difference between examinations was insignificant. They concluded that the DW EPI with 6-values was the most reproducible and that ADC values varied significantly between MRI systems and sequences. Grech-Sollars *et al*[148] (2015) assessed reproducibility of ADC measurements of brain tissue on eight scanners (4 Siemens 1.5T, 4 Philips 3.0T) using an ice-water phantom and 9 healthy volunteers across five institutions. Site-specific clinical protocols were used in this study using a range of *b*-values (0 to 1000 s/mm^2) with additional *b*-values acquired at all centres. All scans were acquired over a period of 18 mo and a total of 65 imaging sessions took place across all centres. Vendor-independent software was used to compute the ADC maps. In the phantom, ADC measurements were reproducible with a CV of less than 1.5%. In the volunteer population, ADC measurements of white and grey matter were reproducible with an inter-scanner CV of 3% and 2.4% and an intra-scanner CV of 1.0% and 2.9% respectively. Overall the authors concluded that using standardized clinical sequences in large multi-centre studies is not essential to achieve good reproducibility of ADC measurements. Winfield *et al*[149] (2015) assessed the effects of eating and fasting on the measured ADCs in livers of 20 healthy volunteers. Four clinical scanners at 3 participating sites from three vendors (1 Philips, 2 Siemens, 1 GE) at 1.5T field strength were used to acquire volunteer data (5 volunteers per scanner). Diffusion weightings of 100, 500 and 900 s/mm^2 were used in this study. Each volunteer was scanned four times, scans 1 and 2 occurring on the same day one with at least four hours of fasting and the other after a meal. These scans were repeated for each volunteer 1-7 d after. Vendor-independent software was used to compute the ADC values at a single site. An ice-water phantom[125] was also used to assess accuracy and repeatability of ADC estimates. Three volunteers were excluded from the final analysis. Coefficient of variation was found to be 5.1% when fasted and 4.6% non-fasted. Between-site CV was found to be 3% using the ice-water phantom. The authors concluded that there was no significant difference in ADC estimates between fasted and non-fasted measurements.

Need for validation

All of the selected studies evaluating ADC repeatability and reproducibility acknowledge that lack of standardization in data analysis, ADC quantification and interpretation is the greatest challenge in the adoption of DW-MRI for tumour assessment[4,5,56]. More studies are emerging focusing on repeatability and reproducibility of ADC measurements across institutions and using MR systems from different vendors. Malyarenko *et al*[150] demonstrated that the measured systematic ADC errors scaled quadratically with offset from a magnet's isocentre. Nonlinearity in the applied diffusion gradients was shown to be a major source of spatial DW bias and variability in off-centre ADC measurements. This bias was found to be dependant on system design and diffusion gradient direction. In the same study, the authors concluded that shim, imaging gradients and eddy currents had minor contributions in the spatial DW bias.

Present post-processing software packages for quantitative DW MRI available on scanner consoles are mostly basic allowing only a mono-exponential fit and some elementary image analysis. Although, the choice of the mathematical model depends on the anatomical region in the study but it is imperative to have the flexibility of using different models as this could influence repeatability. In a recent study on primary and secondary ovarian cancer, a stretched exponential model showed better repeatability over mono-exponential and bi-exponential models[151].

Finally, in any DW-MRI study, system-induced variability must be established using a standardized phantom as was recommended in the 2009 meeting report[5].

DISCUSSION AND CONCLUSION

In this present manuscript ADC values for healthy extracranial organs were summarized. In total 28 studies were selected for liver parenchyma, 15 studies for kidney (renal parenchyma), 14 studies for spleen, 13 for pancreatic body, 6 for gallbladder, 13 for prostate, 13 for uterus (endometrium, myometrium, cervix) and 13 for fibroglandular breast tissue. Median ADC values in selected studies were found to be 1.28×10^{-3} mm^2/s in liver, 1.94×10^{-3} mm^2/s in kidney, 1.60×10^{-3} mm^2/s in pancreatic body, 0.85×10^{-3} mm^2/s in spleen, 2.73×10^{-3}

mm^2/s in gallbladder, 1.64×10^{-3} mm^2/s and 1.31×10^{-3} mm^2/s in prostate peripheral zone and central gland respectively (combined median value of 1.54×10^{-3} mm^2/s), 1.44×10^{-3} mm^2/s in endometrium, 1.53×10^{-3} mm^2/s in myometrium, 1.71×10^{-3} mm^2/s in cervix and 1.92×10^{-3} mm^2/s in breast. Limited studies have assessed ADC of normal uterine tissue particularly myometrium (only 3 data points) which consequently influenced the median ADC value. Differences in reported ADC values are largely attributed to differences in acquisition sequence particularly the choice of *b*-values and the sequence echo-time. More studies are emerging in DW MRI with recommendations on specific *b*-values and protocols that one must adhere to, to interrogate a particular anatomical region. Such studies can be named for liver[23,149], prostate[152] and pancreas[70]. With these organ-specific recommendations, acquisition parameters are becoming more comparable across different studies. Some historical reports of ADC values such as some references in the 1990s and early 2000s must be forgone in favour of more recent reports. Reference ADC values should be derived from a recent study with a recommended set of organ-specific *b*-values or by taking a median of values from multiple studies. Although changes in ADC values has proven to be a diagnostic/prognostic biomarker in differentiating malignant and non-malignant lesions, its value for monitoring response to drug treatment is less established[128]. Braithwaite *et al*[49] demonstrated that treatment effects of less than approximately 27% would not be clinically detectable with confidence with one acquisition in a single individual. Therefore considerable care must be taken in reporting treatment effects based on a single acquisition in a single individual.

Six phantom studies and thirteen *in vivo* studies were summarized in sections "Reproducibility of ADC values *in vitro*" and "Reproducibility of ADC values *in vivo*" to compare repeatability and reproducibility of the measured ADC. All selected phantom studies demonstrated lower intra-scanner and inter-scanner variation compared to *in vivo* studies. To date, very few studies have assessed reproducibility of the measured ADC in extra-cranial body organs. Hence studies assessing reproducibility of head and neck tissue[126,147,148] were also included in this review. Some studies used vendor-independent post-processing software packages to compute the ADC maps[56,125,126,137,140,148] while others used site-specific software packages either vendor-specific or locally developed[68,138,141,147]. Although some investigators demonstrated high variability in the measured ADC (27.1% for left liver lobe) with vendor-independent software packages[56], others found less variability in the measured ADC using vendor-specific software[148]. The majority of investigators found that standardized acquisition protocols improve reproducibility. ADC measurement variability was shown to be higher *in vivo* compared to phantom studies[34,148]. Reproducibility in the measured ADC was also shown to be dependant on the specific anatomy being interrogated[34,56,143]. Whilst a significant variation in the measured ADC of the left hepatic lobe was observed in[56], insignificant variation was observed in the right liver lobe[146].

Larger ROIs[142] and volumetric ROIs[34] demonstrated better reproducibility. Smaller ROIs are also known to suffer from poorer inter- and intra-observer variability[153].

ADC cut-off values are increasingly used in studies to differentiate between normal and cancerous tissues or even between tumour grades. For the latter, the differences between ADC values are often small and, although valid in the populations studied, they should not be taken as absolute numbers and used for diagnosis on a different scanner or with a different imaging protocol. Although variations in ADC values are far greater following treatments one should still be careful when using cut-off values for treatment response. However, assessing treatment response using ADC measures is a promising tool and for example Koh *et al*[154] demonstrated that ADC measurements were highly reproducible with a coefficient of repeatability of 0.17 in a two-centre phase 1 clinical trial setting.

Recommendations

Protocol needs to be optimised for the body part studied.

System-induced variability must be established using a standardized phantom in any clinical study.

Reproducibility of the measured ADC must be assessed in a volunteer population, as variations are far more significant *in vivo* compared with phantom studies.

Studies need to be assessed properly; acquisition parameters across participating sites/scanners must be matched as best as possible, in particular *b*-values, TE and bandwidth.

Evaluation must be organ-specific and ROI size must be taken into consideration.

Recommended statistical tests to assess repeatability and reproducibility must be utilized for a credible investigator report.

REFERENCES

1 **Le Bihan D**, Breton E, Lallemand D, Grenier P, Cabanis E, Laval-Jeantet M. MR imaging of intravoxel incoherent motions: application to diffusion and perfusion in neurologic disorders. *Radiology* 1986; **161**: 401-407 [PMID: 3763909 DOI: 10.1148/radiology.161.2.3763909]

2 **Warach S**, Chien D, Li W, Ronthal M, Edelman RR. Fast magnetic resonance diffusion-weighted imaging of acute human stroke. *Neurology* 1992; **42**: 1717-1723 [PMID: 1513459]

3 **Le Bihan D**. Intravoxel incoherent motion perfusion MR imaging: a wake-up call. *Radiology* 2008; **249**: 748-752 [PMID: 19011179 DOI: 10.1148/radiol.2493081301]

4 **Koh DM**, Collins DJ. Diffusion-weighted MRI in the body: applications and challenges in oncology. *AJR Am J Roentgenol* 2007; **188**: 1622-1635 [PMID: 17515386 DOI: 10.2214/AJR.06.1403]

5 **Padhani AR**, Liu G, Koh DM, Chenevert TL, Thoeny HC, Takahara T, Dzik-Jurasz A, Ross BD, Van Cauteren M, Collins D, Hammoud DA, Rustin GJ, Taouli B, Choyke PL. Diffusion-weighted magnetic resonance imaging as a cancer biomarker: consensus and recommendations. *Neoplasia* 2009; **11**: 102-125 [PMID: 19186405 DOI: 10.1593/neo.81328]

6 **Einstein A**. Uber die von der molekularkinetischen Theorie der Warme geforderte Bewegung von in ruhenden Flussigkeiten

suspendierten Teilchen. *Annalen der Physik* 1905; **322**: 549-560 [DOI: 10.1002/andp.19053220806]
7 **Mills R**. Self-diffusion In Normal and Heavy-water In Range 1-45 Degrees. *J Phys Chem* 1973; **77**: 685-688 [DOI: 10.1021/j100624a025]
8 **Le Bihan D**, Breton E, Lallemand D, Aubin ML, Vignaud J, Laval-Jeantet M. Separation of diffusion and perfusion in intravoxel incoherent motion MR imaging. *Radiology* 1988; **168**: 497-505 [PMID: 3393671 DOI: 10.1148/radiology.168.2.3393671]
9 **Price WS**. Pulsed-field gradient nuclear magnetic resonance as a tool for studying translational diffusion.1. Basic theory. *Concepts In Magnetic Resonance* 1997; **9**: 299-336 [DOI: 10.1002/(SICI)1099-0534(1997)9:5<299::AID-CMR2>3.0.CO;2-U]
10 **Stejskal EO**. Use of Spin Echoes in a Pulsed Magnetic-Field Gradient to Study Anisotropic, Restricted Diffusion and Flow. *J Phys Chem* 1965: **43**: 3597-3603 [DOI: 10.1063/1.1696526]
11 **Tanner JE**. Use of the Stimulated Echo in NMR Diffusion Studies. *J Phys Chem* 1970; **52**: 2523-2526 [DOI: 10.1063/1.1673336]
12 **Merboldt KD**, Hänicke W, Bruhn H, Gyngell ML, Frahm J. Diffusion imaging of the human brain in vivo using high-speed STEAM MRI. *Magn Reson Med* 1992; **23**: 179-192 [PMID: 1734178 DOI: 10.1002/mrm.1910230119]
13 **Le Bihan D**. Intravoxel incoherent motion imaging using steady-state free precession. *Magn Reson Med* 1988; **7**: 346-351 [PMID: 3205150 DOI: 10.1002/mrm.1910070312]
14 **Baur A**, Stäbler A, Brüning R, Bartl R, Krödel A, Reiser M, Deimling M. Diffusion-weighted MR imaging of bone marrow: differentiation of benign versus pathologic compression fractures. *Radiology* 1998; **207**: 349-356 [PMID: 9577479 DOI: 10.1148/radiology.207.2.9577479]
15 **McNab JA**, Jbabdi S, Deoni SC, Douaud G, Behrens TE, Miller KL. High resolution diffusion-weighted imaging in fixed human brain using diffusion-weighted steady state free precession. *Neuroimage* 2009; **46**: 775-785 [PMID: 19344686 DOI: 10.1016/j.neuroimage.2009.01.008]
16 **Patterson DM**, Padhani AR, Collins DJ. Technology insight: water diffusion MRI--a potential new biomarker of response to cancer therapy. *Nat Clin Pract Oncol* 2008; **5**: 220-233 [PMID: 18301415 DOI: 10.1038/ncponc1073]
17 **Partridge SC**, McKinnon GC, Henry RG, Hylton NM. Menstrual cycle variation of apparent diffusion coefficients measured in the normal breast using MRI. *J Magn Reson Imaging* 2001; **14**: 433-438 [PMID: 11599068 DOI: 10.1002/jmri.1204]
18 **Chenevert TL**, Malyarenko DI, Newitt D, Li X, Jayatilake M, Tudorica A, Fedorov A, Kikinis R, Liu TT, Muzi M, Oborski MJ, Laymon CM, Li X, Thomas Y, Jayashree KC, Mountz JM, Kinahan PE, Rubin DL, Fennessy F, Huang W, Hylton N, Ross BD. Errors in Quantitative Image Analysis due to Platform-Dependent Image Scaling. *Transl Oncol* 2014; **7**: 65-71 [PMID: 24772209 DOI: 10.1593/tlo.13811]
19 **Koh DM**, Collins DJ, Orton MR. Intravoxel incoherent motion in body diffusion-weighted MRI: reality and challenges. *AJR Am J Roentgenol* 2011; **196**: 1351-1361 [PMID: 21606299 DOI: 10.2214/AJR.10.5515]
20 **Bennett KM**, Schmainda KM, Bennett RT, Rowe DB, Lu H, Hyde JS. Characterization of continuously distributed cortical water diffusion rates with a stretched-exponential model. *Magn Reson Med* 2003; **50**: 727-734 [PMID: 14523958 DOI: 10.1002/mrm.10581]
21 **Yablonskiy DA**, Bretthorst GL, Ackerman JJ. Statistical model for diffusion attenuated MR signal. *Magn Reson Med* 2003; **50**: 664-669 [PMID: 14523949 DOI: 10.1002/mrm.10578]
22 **Jensen JH**, Helpern JA, Ramani A, Lu H, Kaczynski K. Diffusional kurtosis imaging: the quantification of non-gaussian water diffusion by means of magnetic resonance imaging. *Magn Reson Med* 2005; **53**: 1432-1440 [PMID: 15906300 DOI: 10.1002/mrm.20508]
23 **Taouli B**, Koh DM. Diffusion-weighted MR imaging of the liver. *Radiology* 2010; **254**: 47-66 [PMID: 20032142 DOI: 10.1148/radiol.09090021]
24 **Yamada I**, Aung W, Himeno Y, Nakagawa T, Shibuya H. Diffusion coefficients in abdominal organs and hepatic lesions: evaluation with intravoxel incoherent motion echo-planar MR imaging. *Radiology* 1999; **210**: 617-623 [PMID: 10207458 DOI: 10.1148/radiology.210.3.r99fe17617]
25 **Moteki T**, Horikoshi H, Oya N, Aoki J, Endo K. Evaluation of hepatic lesions and hepatic parenchyma using diffusion-weighted reordered turboFLASH magnetic resonance images. *J Magn Reson Imaging* 2002; **15**: 564-572 [PMID: 11997898 DOI: 10.1002/jmri.10101]
26 **Quentin M**, Blondin D, Klasen J, Lanzman RS, Miese FR, Arsov C, Albers P, Antoch G, Wittsack HJ. Comparison of different mathematical models of diffusion-weighted prostate MR imaging. *Magn Reson Imaging* 2012; **30**: 1468-1474 [PMID: 22819178 DOI: 10.1016/j.mri.2012.04.025]
27 **Riches SF**, Hawtin K, Charles-Edwards EM, de Souza NM. Diffusion-weighted imaging of the prostate and rectal wall: comparison of biexponential and monoexponential modelled diffusion and associated perfusion coefficients. *NMR Biomed* 2009; **22**: 318-325 [PMID: 19009566 DOI: 10.1002/nbm.1328]
28 **Ichikawa T**, Haradome H, Hachiya J, Nitatori T, Araki T. Diffusion-weighted MR imaging with a single-shot echoplanar sequence: detection and characterization of focal hepatic lesions. *AJR Am J Roentgenol* 1998; **170**: 397-402 [PMID: 9456953 DOI: 10.2214/ajr.170.2.9456953]
29 **Kim T**, Murakami T, Takahashi S, Hori M, Tsuda K, Nakamura H. Diffusion-weighted single-shot echoplanar MR imaging for liver disease. *AJR Am J Roentgenol* 1999; **173**: 393-398 [PMID: 10430143 DOI: 10.2214/ajr.173.2.10430143]
30 **Namimoto T**, Yamashita Y, Mitsuzaki K, Nakayama Y, Tang Y, Takahashi M. Measurement of the apparent diffusion coefficient in diffuse renal disease by diffusion-weighted echo-planar MR imaging. *J Magn Reson Imaging* 1999; **9**: 832-837 [PMID: 10373031 DOI: 10.1002/(SICI)1522-2586(199906)9:6<832::AID-JMRI13>3.0.CO;2-1]
31 **Thoeny HC**, De Keyzer F, Oyen RH, Peeters RR. Diffusion-weighted MR imaging of kidneys in healthy volunteers and patients with parenchymal diseases: initial experience. *Radiology* 2005; **235**: 911-917 [PMID: 15845792 DOI: 10.1148/radiol.2353040554]
32 **Mürtz P**, Flacke S, Träber F, van den Brink JS, Gieseke J, Schild HH. Abdomen: diffusion-weighted MR imaging with pulse-triggered single-shot sequences. *Radiology* 2002; **224**: 258-264 [PMID: 12091693 DOI: 10.1148/radiol.2241011117]
33 **Leporq B**, Saint-Jalmes H, Rabrait C, Pilleul F, Guillaud O, Dumortier J, Scoazec JY, Beuf O. Optimization of intra-voxel incoherent motion imaging at 3.0 Tesla for fast liver examination. *J Magn Reson Imaging* 2015; **41**: 1209-1217 [PMID: 25044653 DOI: 10.1002/jmri.24693]
34 **Miquel ME**, Scott AD, Macdougall ND, Boubertakh R, Bharwani N, Rockall AG. In vitro and in vivo repeatability of abdominal diffusion-weighted MRI. *Br J Radiol* 2012; **85**: 1507-1512 [PMID: 22674704 DOI: 10.1259/bjr/32269440]
35 **Duran R**, Ronot M, Kerbaol A, Van Beers B, Vilgrain V. Hepatic hemangiomas: factors associated with T2 shine-through effect on diffusion-weighted MR sequences. *Eur J Radiol* 2014; **83**: 468-478 [PMID: 24364922 DOI: 10.1016/j.ejrad.2013.11.023]
36 **Burdette JH**, Elster AD, Ricci PE. Acute cerebral infarction: quantification of spin-density and T2 shine-through phenomena on diffusion-weighted MR images. *Radiology* 1999; **212**: 333-339 [PMID: 10429687 DOI: 10.1148/radiology.212.2.r99au36333]
37 **Pierpaoli C**, Jezzard P, Basser PJ, Barnett A, Di Chiro G. Diffusion tensor MR imaging of the human brain. *Radiology* 1996; **201**: 637-648 [PMID: 8939209 DOI: 10.1148/radiology.201.3.8939209]
38 **Le Bihan D**, Mangin JF, Poupon C, Clark CA, Pappata S, Molko N, Chabriat H. Diffusion tensor imaging: concepts and applications. *J Magn Reson Imaging* 2001; **13**: 534-546 [PMID: 11276097 DOI: 10.1002/jmri.1076]
39 **Taouli B**, Martin AJ, Qayyum A, Merriman RB, Vigneron D, Yeh BM, Coakley FV. Parallel imaging and diffusion tensor imaging for diffusion-weighted MRI of the liver: preliminary experience in healthy volunteers. *AJR Am J Roentgenol* 2004; **183**: 677-680

[PMID: 15333355 DOI: 10.2214/ajr.183.3.1830677]
40 **Tosun M**, Inan N, Sarisoy HT, Akansel G, Gumustas S, Gürbüz Y, Demirci A. Diagnostic performance of conventional diffusion weighted imaging and diffusion tensor imaging for the liver fibrosis and inflammation. *Eur J Radiol* 2013; **82**: 203-207 [PMID: 23122674 DOI: 10.1016/j.ejrad.2012.09.009]
41 **Ries M**, Jones RA, Basseau F, Moonen CT, Grenier N. Diffusion tensor MRI of the human kidney. *J Magn Reson Imaging* 2001; **14**: 42-49 [PMID: 11436213 DOI: 10.1002/jmri.1149]
42 **Notohamiprodjo M**, Glaser C, Herrmann KA, Dietrich O, Attenberger UI, Reiser MF, Schoenberg SO, Michaely HJ. Diffusion tensor imaging of the kidney with parallel imaging: initial clinical experience. *Invest Radiol* 2008; **43**: 677-685 [PMID: 18791409 DOI: 10.1097/RLI.0b013e31817d14e6]
43 **Notohamiprodjo M**, Dietrich O, Horger W, Horng A, Helck AD, Herrmann KA, Reiser MF, Glaser C. Diffusion tensor imaging (DTI) of the kidney at 3 tesla-feasibility, protocol evaluation and comparison to 1.5 Tesla. *Invest Radiol* 2010; **45**: 245-254 [PMID: 20375845 DOI: 10.1097/RLI.0b013e3181d83abc]
44 **Partridge SC**, Murthy RS, Ziadloo A, White SW, Allison KH, Lehman CD. Diffusion tensor magnetic resonance imaging of the normal breast. *Magn Reson Imaging* 2010; **28**: 320-328 [PMID: 20061111 DOI: 10.1016/j.mri.2009.10.003]
45 **Gürses B**, Kabakci N, Kovanlikaya A, Firat Z, Bayram A, Uluğ AM, Kovanlikaya I. Diffusion tensor imaging of the normal prostate at 3 Tesla. *Eur Radiol* 2008; **18**: 716-721 [PMID: 17960389 DOI: 10.1007/s00330-007-0795-7]
46 **Bonekamp S**, Corona-Villalobos CP, Kamel IR. Oncologic applications of diffusion-weighted MRI in the body. *J Magn Reson Imaging* 2012; **35**: 257-279 [PMID: 22271274 DOI: 10.1002/jmri.22786]
47 **Taouli B**, Vilgrain V, Dumont E, Daire JL, Fan B, Menu Y. Evaluation of liver diffusion isotropy and characterization of focal hepatic lesions with two single-shot echo-planar MR imaging sequences: prospective study in 66 patients. *Radiology* 2003; **226**: 71-78 [PMID: 12511671 DOI: 10.1148/radiol.2261011904]
48 **Larsen NE**, Haack S, Larsen LP, Pedersen EM. Quantitative liver ADC measurements using diffusion-weighted MRI at 3 Tesla: evaluation of reproducibility and perfusion dependence using different techniques for respiratory compensation. *MAGMA* 2013; **26**: 431-442 [PMID: 23483359 DOI: 10.1007/s10334-013-0375-6]
49 **Braithwaite AC**, Dale BM, Boll DT, Merkle EM. Short- and midterm reproducibility of apparent diffusion coefficient measurements at 3.0-T diffusion-weighted imaging of the abdomen. *Radiology* 2009; **250**: 459-465 [PMID: 19095786 DOI: 10.1148/radiol.2502080849]
50 **de Bazelaire CM**, Duhamel GD, Rofsky NM, Alsop DC. MR imaging relaxation times of abdominal and pelvic tissues measured in vivo at 3.0 T: preliminary results. *Radiology* 2004; **230**: 652-659 [PMID: 14990831 DOI: 10.1148/radiol.2303021331]
51 **Watanabe H**, Kanematsu M, Goshima S, Kondo H, Onozuka M, Moriyama N, Bae KT. Staging hepatic fibrosis: comparison of gadoxetate disodium-enhanced and diffusion-weighted MR imaging--preliminary observations. *Radiology* 2011; **259**: 142-150 [PMID: 21248234 DOI: 10.1148/radiol.10100621]
52 **Kenis C**, Deckers F, De Foer B, Van Mieghem F, Van Laere S, Pouillon M. Diagnosis of liver metastases: can diffusion-weighted imaging (DWI) be used as a stand alone sequence? *Eur J Radiol* 2012; **81**: 1016-1023 [PMID: 21377305 DOI: 10.1016/j.ejrad.2011.02.019]
53 **Guo W**, Zhao S, Yang Y, Shao G. Histological grade of hepatocellular carcinoma predicted by quantitative diffusion-weighted imaging. *Int J Clin Exp Med* 2015; **8**: 4164-4169 [PMID: 26064326]
54 **Nasu K**, Kuroki Y, Tsukamoto T, Nakajima H, Mori K, Minami M. Diffusion-weighted imaging of surgically resected hepatocellular carcinoma: imaging characteristics and relationship among signal intensity, apparent diffusion coefficient, and histopathologic grade. *AJR Am J Roentgenol* 2009; **193**: 438-444 [PMID: 19620441 DOI: 10.2214/AJR.08.1424]
55 **Chow LC**, Bammer R, Moseley ME, Sommer FG. Single breath-hold diffusion-weighted imaging of the abdomen. *J Magn Reson Imaging* 2003; **18**: 377-382 [PMID: 12938137 DOI: 10.1002/jmri.10353]
56 **Donati OF**, Chong D, Nanz D, Boss A, Froehlich JM, Andres E, Seifert B, Thoeny HC. Diffusion-weighted MR imaging of upper abdominal organs: field strength and intervendor variability of apparent diffusion coefficients. *Radiology* 2014; **270**: 454-463 [PMID: 24471390 DOI: 10.1148/radiol.13130819]
57 **Yoshikawa T**, Kawamitsu H, Mitchell DG, Ohno Y, Ku Y, Seo Y, Fujii M, Sugimura K. ADC measurement of abdominal organs and lesions using parallel imaging technique. *AJR Am J Roentgenol* 2006; **187**: 1521-1530 [PMID: 17114546 DOI: 10.2214/AJR.05.0778]
58 **Corona-Villalobos CP**, Pan L, Halappa VG, Bonekamp S, Lorenz CH, Eng J, Kamel IR. Agreement and reproducibility of apparent diffusion coefficient measurements of dual-b-value and multi-b-value diffusion-weighted magnetic resonance imaging at 1.5 Tesla in phantom and in soft tissues of the abdomen. *J Comput Assist Tomogr* 2013; **37**: 46-51 [PMID: 23321832 DOI: 10.1097/RCT.0b013e3182720e07]
59 **Fukuda Y**, Ohashi I, Hanafusa K, Nakagawa T, Ohtani S, An-naka Y, Hayashi T, Shibuya H. Anisotropic diffusion in kidney: apparent diffusion coefficient measurements for clinical use. *J Magn Reson Imaging* 2000; **11**: 156-160 [PMID: 10713948 DOI: 10.1002/(SICI)1522-2586(200002)11:2<156::AID-JMRI12>3.0.CO;2-8]
60 **Müller MF**, Prasad P, Siewert B, Nissenbaum MA, Raptopoulos V, Edelman RR. Abdominal diffusion mapping with use of a whole-body echo-planar system. *Radiology* 1994; **190**: 475-478 [PMID: 8284402 DOI: 10.1148/radiology.190.2.8284402]
61 **Morani AC**, Elsayes KM, Liu PS, Weadock WJ, Szklaruk J, Dillman JR, Khan A, Chenevert TL, Hussain HK. Abdominal applications of diffusion-weighted magnetic resonance imaging: Where do we stand. *World J Radiol* 2013; **5**: 68-80 [PMID: 23671743 DOI: 10.4329/wjr.v5.i3.68]
62 **Papanikolaou N**, Gourtsoyianni S, Yarmenitis S, Maris T, Gourtsoyiannis N. Comparison between two-point and four-point methods for quantification of apparent diffusion coefficient of normal liver parenchyma and focal lesions. Value of normalization with spleen. *Eur J Radiol* 2010; **73**: 305-309 [PMID: 19091503 DOI: 10.1016/j.ejrad.2008.10.023]
63 **Klasen J**, Lanzman RS, Wittsack HJ, Kircheis G, Schek J, Quentin M, Antoch G, Häussinger D, Blondin D. Diffusion-weighted imaging (DWI) of the spleen in patients with liver cirrhosis and portal hypertension. *Magn Reson Imaging* 2013; **31**: 1092-1096 [PMID: 23731536 DOI: 10.1016/j.mri.2013.01.003]
64 **Kiliçkesmez O**, Yirik G, Bayramoğlu S, Cimilli T, Aydin S. Non-breath-hold high b-value diffusion-weighted MRI with parallel imaging technique: apparent diffusion coefficient determination in normal abdominal organs. *Diagn Interv Radiol* 2008; **14**: 83-87 [PMID: 18553281]
65 **Fattahi R**, Balci NC, Perman WH, Hsueh EC, Alkaade S, Havlioglu N, Burton FR. Pancreatic diffusion-weighted imaging (DWI): comparison between mass-forming focal pancreatitis (FP), pancreatic cancer (PC), and normal pancreas. *J Magn Reson Imaging* 2009; **29**: 350-356 [PMID: 19161187 DOI: 10.1002/jmri.21651]
66 **Cho SG**, Lee DH, Lee KY, Ji H, Lee KH, Ros PR, Suh CH. Differentiation of chronic focal pancreatitis from pancreatic carcinoma by in vivo proton magnetic resonance spectroscopy. *J Comput Assist Tomogr* 2005; **29**: 163-169 [PMID: 15772531 DOI: 10.1097/01.rct.0000153956.33296.b5]
67 **Kim JK**, Altun E, Elias J, Pamuklar E, Rivero H, Semelka RC. Focal pancreatic mass: distinction of pancreatic cancer from chronic pancreatitis using gadolinium-enhanced 3D-gradient-echo MRI. *J Magn Reson Imaging* 2007; **26**: 313-322 [PMID: 17610286 DOI: 10.1002/jmri.21010]
68 **Barral M**, Soyer P, Ben Hassen W, Gayat E, Aout M, Chiaradia M, Rahmouni A, Luciani A. Diffusion-weighted MR imaging of the normal pancreas: reproducibility and variations of apparent diffusion coefficient measurement at 1.5- and 3.0-Tesla. *Diagn*

Interv Imaging 2013; **94**: 418-427 [PMID: 23415463 DOI: 10.1016/j.diii.2012.12.007]

69 **Ichikawa T**, Erturk SM, Motosugi U, Sou H, Iino H, Araki T, Fujii H. High-b value diffusion-weighted MRI for detecting pancreatic adenocarcinoma: preliminary results. *AJR Am J Roentgenol* 2007; **188**: 409-414 [PMID: 17242249 DOI: 10.2214/AJR.05.1918]

70 **Barral M**, Taouli B, Guiu B, Koh DM, Luciani A, Manfredi R, Vilgrain V, Hoeffel C, Kanematsu M, Soyer P. Diffusion-weighted MR imaging of the pancreas: current status and recommendations. *Radiology* 2015; **274**: 45-63 [PMID: 25531479 DOI: 10.1148/radiol.14130778]

71 **Lee NK**, Kim S, Kim TU, Kim DU, Seo HI, Jeon TY. Diffusion-weighted MRI for differentiation of benign from malignant lesions in the gallbladder. *Clin Radiol* 2014; **69**: e78-e85 [PMID: 24290779 DOI: 10.1016/j.crad.2013.09.017]

72 **Yeh BM**, Liu PS, Soto JA, Corvera CA, Hussain HK. MR imaging and CT of the biliary tract. *Radiographics* 2009; **29**: 1669-1688 [PMID: 19959515 DOI: 10.1148/rg.296095514]

73 **Le Bihan D**, Delannoy J, Levin RL. Temperature mapping with MR imaging of molecular diffusion: application to hyperthermia. *Radiology* 1989; **171**: 853-857 [PMID: 2717764 DOI: 10.1148/radiology.171.3.2717764]

74 **Emad-Eldin S**, Halim M, Metwally LIA, Abdel-Aziz RM. Diffusion-weighted MR imaging and ADC measurement in normal prostate, benign prostatic hyperplasia and prostate carcinoma. *ESRNM* 2014: **45**: 535-542 [DOI: 10.1016/j.ejrnm.2014.02.017]

75 **Anderson AW**, Xie J, Pizzonia J, Bronen RA, Spencer DD, Gore JC. Effects of cell volume fraction changes on apparent diffusion in human cells. *Magn Reson Imaging* 2000; **18**: 689-695 [PMID: 10930778 DOI: 10.1016/S0730-725X(00)00147-8]

76 **Kozlowski P**, Chang SD, Goldenberg SL. Diffusion-weighted MRI in prostate cancer -- comparison between single-shot fast spin echo and echo planar imaging sequences. *Magn Reson Imaging* 2008; **26**: 72-76 [PMID: 17566687 DOI: 10.1016/j.mri.2007.04.008]

77 **Gibbs P**, Tozer DJ, Liney GP, Turnbull LW. Comparison of quantitative T2 mapping and diffusion-weighted imaging in the normal and pathologic prostate. *Magn Reson Med* 2001; **46**: 1054-1058 [PMID: 11746568 DOI: 10.1002/mrm.1298]

78 **Kumar V**, Jagannathan NR, Kumar R, Das SC, Jindal L, Thulkar S, Gupta SD, Dwivedi SN, Roell S, Hemal AK, Gupta NP. Correlation between metabolite ratios and ADC values of prostate in men with increased PSA level. *Magn Reson Imaging* 2006; **24**: 541-548 [PMID: 16735174 DOI: 10.1016/j.mri.2006.01.001]

79 **Sato C**, Naganawa S, Nakamura T, Kumada H, Miura S, Takizawa O, Ishigaki T. Differentiation of noncancerous tissue and cancer lesions by apparent diffusion coefficient values in transition and peripheral zones of the prostate. *J Magn Reson Imaging* 2005; **21**: 258-262 [PMID: 15723379 DOI: 10.1002/jmri.20251]

80 **Haider MA**, van der Kwast TH, Tanguay J, Evans AJ, Hashmi AT, Lockwood G, Trachtenberg J. Combined T2-weighted and diffusion-weighted MRI for localization of prostate cancer. *AJR Am J Roentgenol* 2007; **189**: 323-328 [PMID: 17646457 DOI: 10.2214/AJR.07.2211]

81 **ACR**. Prostate imaging reporting and data system (PIRADS). American College of Radiology, 2015; 2: 66. Available from: URL: http://www.acr.org/~/media/ACR/Documents/PDF/QualitySafety/Resources/PIRADS/PIRADS V2.pdf

82 **McNeal JE**, Redwine EA, Freiha FS, Stamey TA. Zonal distribution of prostatic adenocarcinoma. Correlation with histologic pattern and direction of spread. *Am J Surg Pathol* 1988; **12**: 897-906 [PMID: 3202246 DOI: 10.1097/00000478-198812000-00001]

83 **Malayeri AA**, El Khouli RH, Zaheer A, Jacobs MA, Corona-Villalobos CP, Kamel IR, Macura KJ. Principles and applications of diffusion-weighted imaging in cancer detection, staging, and treatment follow-up. *Radiographics* 2011; **31**: 1773-1791 [PMID: 21997994 DOI: 10.1148/rg.316115515]

84 **Park BK**, Lee HM, Kim CK, Choi HY, Park JW. Lesion localization in patients with a previous negative transrectal ultrasound biopsy and persistently elevated prostate specific antigen level using diffusion-weighted imaging at three Tesla before rebiopsy. *Invest Radiol* 2008; **43**: 789-793 [PMID: 18923258 DOI: 10.1097/RLI.0b013e318183725e]

85 **Wakefield JC**, Downey K, Kyriazi S, deSouza NM. New MR techniques in gynecologic cancer. *AJR Am J Roentgenol* 2013; **200**: 249-260 [PMID: 23345344 DOI: 10.2214/AJR.12.8932]

86 **Namimoto T**, Awai K, Nakaura T, Yanaga Y, Hirai T, Yamashita Y. Role of diffusion-weighted imaging in the diagnosis of gynecological diseases. *Eur Radiol* 2009; **19**: 745-760 [PMID: 18839179 DOI: 10.1007/s00330-008-1185-5]

87 **Cao K**, Gao M, Sun YS, Li YL, Sun Y, Gao YN, Zhang XP. Apparent diffusion coefficient of diffusion weighted MRI in endometrial carcinoma-Relationship with local invasiveness. *Eur J Radiol* 2012; **81**: 1926-1930 [PMID: 21592709 DOI: 10.1016/j.ejrad.2011.04.019]

88 **Tamai K**, Koyama T, Saga T, Umeoka S, Mikami Y, Fujii S, Togashi K. Diffusion-weighted MR imaging of uterine endometrial cancer. *J Magn Reson Imaging* 2007; **26**: 682-687 [PMID: 17729360 DOI: 10.1002/jmri.20997]

89 **Tamai K**, Koyama T, Saga T, Morisawa N, Fujimoto K, Mikami Y, Togashi K. The utility of diffusion-weighted MR imaging for differentiating uterine sarcomas from benign leiomyomas. *Eur Radiol* 2008; **18**: 723-730 [PMID: 17929022 DOI: 10.1007/s00330-007-0787-7]

90 **Kuang F**, Ren J, Zhong Q, Liyuan F, Huan Y, Chen Z. The value of apparent diffusion coefficient in the assessment of cervical cancer. *Eur Radiol* 2013; **23**: 1050-1058 [PMID: 23179520 DOI: 10.1007/s00330-012-2681-1]

91 **McVeigh PZ**, Syed AM, Milosevic M, Fyles A, Haider MA. Diffusion-weighted MRI in cervical cancer. *Eur Radiol* 2008; **18**: 1058-1064 [PMID: 18193428 DOI: 10.1007/s00330-007-0843-3]

92 **Shen SH**, Chiou YY, Wang JH, Yen MS, Lee RC, Lai CR, Chang CY. Diffusion-weighted single-shot echo-planar imaging with parallel technique in assessment of endometrial cancer. *AJR Am J Roentgenol* 2008; **190**: 481-488 [PMID: 18212236 DOI: 10.2214/AJR.07.2155]

93 **Nougaret S**, Reinhold C, Alsharif SS, Addley H, Arceneau J, Molinari N, Guiu B, Sala E. Endometrial Cancer: Combined MR Volumetry and Diffusion-weighted Imaging for Assessment of Myometrial and Lymphovascular Invasion and Tumor Grade. *Radiology* 2015; **276**: 797-808 [PMID: 25928157 DOI: 10.1148/radiol.15141212]

94 **Levy A**, Medjhoul A, Caramella C, Zareski E, Berges O, Chargari C, Boulet B, Bidault F, Dromain C, Balleyguier C. Interest of diffusion-weighted echo-planar MR imaging and apparent diffusion coefficient mapping in gynecological malignancies: a review. *J Magn Reson Imaging* 2011; **33**: 1020-1027 [PMID: 21509857 DOI: 10.1002/jmri.22546]

95 **Katayama M**, Masui T, Kobayashi S, Ito T, Sakahara H, Nozaki A, Kabasawa H. Diffusion-weighted echo planar imaging of ovarian tumors: is it useful to measure apparent diffusion coefficients? *J Comput Assist Tomogr* 2002; **26**: 250-256 [PMID: 11884782 DOI: 10.1097/00004728-200203000-00015]

96 **Takeuchi M**, Matsuzaki K, Nishitani H. Diffusion-weighted magnetic resonance imaging of endometrial cancer: differentiation from benign endometrial lesions and preoperative assessment of myometrial invasion. *Acta Radiol* 2009; **50**: 947-953 [PMID: 19724949 DOI: 10.1080/02841850903099981]

97 **Takeuchi M**, Matsuzaki K, Nishitani H. Diffusion-weighted magnetic resonance imaging of ovarian tumors: differentiation of benign and malignant solid components of ovarian masses. *J Comput Assist Tomogr* 2010; **34**: 173-176 [PMID: 20351498 DOI: 10.1097/RCT.0b013e3181c2f0a2]

98 **Chen J**, Zhang Y, Liang B, Yang Z. The utility of diffusion-weighted MR imaging in cervical cancer. *Eur J Radiol* 2010; **74**: e101-e106 [PMID: 19442466 DOI: 10.1016/j.ejrad.2009.04.025]

99 **Naganawa S**, Sato C, Kumada H, Ishigaki T, Miura S, Takizawa O. Apparent diffusion coefficient in cervical cancer of the uterus: comparison with the normal uterine cervix. *Eur Radiol* 2005; **15**: 71-78 [PMID: 15538578 DOI: 10.1007/s00330-004-2529-4]

100 **Luomaranta A**, Leminen A, Loukovaara M. Magnetic resonance

imaging in the assessment of high-risk features of endometrial carcinoma: a meta-analysis. *Int J Gynecol Cancer* 2015; **25**: 837-842 [PMID: 25010040 DOI: 10.1097/IGC.0000000000000194]

101 **Leach MO**, Boggis CR, Dixon AK, Easton DF, Eeles RA, Evans DG, Gilbert FJ, Griebsch I, Hoff RJ, Kessar P, Lakhani SR, Moss SM, Nerurkar A, Padhani AR, Pointon LJ, Thompson D, Warren RM. Screening with magnetic resonance imaging and mammography of a UK population at high familial risk of breast cancer: a prospective multicentre cohort study (MARIBS). *Lancet* 2005; **365**: 1769-1778 [PMID: 15910949 DOI: 10.1016/S0140-6736(05)66481-1]

102 **Saslow D**, Boetes C, Burke W, Harms S, Leach MO, Lehman CD, Morris E, Pisano E, Schnall M, Sener S, Smith RA, Warner E, Yaffe M, Andrews KS, Russell CA. American Cancer Society guidelines for breast screening with MRI as an adjunct to mammography. *CA Cancer J Clin* 2007; **57**: 75-89 [PMID: 17392385]

103 **Sardanelli F**, Giuseppetti GM, Panizza P, Bazzocchi M, Fausto A, Simonetti G, Lattanzio V, Del Maschio A. Sensitivity of MRI versus mammography for detecting foci of multifocal, multicentric breast cancer in Fatty and dense breasts using the whole-breast pathologic examination as a gold standard. *AJR Am J Roentgenol* 2004; **183**: 1149-1157 [PMID: 15385322 DOI: 10.2214/ajr.183.4.1831149]

104 **O'Flynn EA**, Wilson RM, Allen SD, Locke I, Scurr E, deSouza NM. Diffusion-weighted imaging of the high-risk breast: Apparent diffusion coefficient values and their relationship to breast density. *J Magn Reson Imaging* 2014; **39**: 805-811 [PMID: 24038529 DOI: 10.1002/jmri.24243]

105 **Sinha S**, Lucas-Quesada FA, Sinha U, DeBruhl N, Bassett LW. In vivo diffusion-weighted MRI of the breast: potential for lesion characterization. *J Magn Reson Imaging* 2002; **15**: 693-704 [PMID: 12112520 DOI: 10.1002/jmri.10116]

106 **Woodhams R**, Matsunaga K, Kan S, Hata H, Ozaki M, Iwabuchi K, Kuranami M, Watanabe M, Hayakawa K. ADC mapping of benign and malignant breast tumors. *Magn Reson Med Sci* 2005; **4**: 35-42 [PMID: 16127252 DOI: 10.2463/mrms.4.35]

107 **Yoshikawa MI**, Ohsumi S, Sugata S, Kataoka M, Takashima S, Mochizuki T, Ikura H, Imai Y. Relation between cancer cellularity and apparent diffusion coefficient values using diffusion-weighted magnetic resonance imaging in breast cancer. *Radiat Med* 2008; **26**: 222-226 [PMID: 18509722 DOI: 10.1007/s11604-007-0218-3]

108 **Al Rashidi N**, Waiter G, Redpath T, Gilbert FJ. Assessment of the apparent diffusion coefficient (ADC) of normal breast tissue during the menstrual cycle at 3T using image segmentation. *Eur J Radiol* 2012; **81** Suppl 1: S1-S3 [PMID: 23083544 DOI: 10.1016/S0720-048X(12)70001-3]

109 **O'Flynn EA**, Morgan VA, Giles SL, deSouza NM. Diffusion weighted imaging of the normal breast: reproducibility of apparent diffusion coefficient measurements and variation with menstrual cycle and menopausal status. *Eur Radiol* 2012; **22**: 1512-1518 [PMID: 22367471 DOI: 10.1007/s00330-012-2399-0]

110 **Graham SJ**, Ness S, Hamilton BS, Bronskill MJ. Magnetic resonance properties of ex vivo breast tissue at 1.5 T. *Magn Reson Med* 1997; **38**: 669-677 [PMID: 9324335 DOI: 10.1002/mrm.1910380422]

111 **Woodhams R**, Ramadan S, Stanwell P, Sakamoto S, Hata H, Ozaki M, Kan S, Inoue Y. Diffusion-weighted imaging of the breast: principles and clinical applications. *Radiographics* 2011; **31**: 1059-1084 [PMID: 21768239 DOI: 10.1148/rg.314105160]

112 **Wenkel E**, Geppert C, Schulz-Wendtland R, Uder M, Kiefer B, Bautz W, Janka R. Diffusion weighted imaging in breast MRI: comparison of two different pulse sequences. *Acad Radiol* 2007; **14**: 1077-1083 [PMID: 17707315 DOI: 10.1016/j.acra.2007.06.006]

113 **Kazama T**, Nasu K, Kuroki Y, Nawano S, Ito H. Comparison of diffusion-weighted images using short inversion time inversion recovery or chemical shift selective pulse as fat suppression in patients with breast cancer. *Jpn J Radiol* 2009; **27**: 163-167 [PMID: 19499306 DOI: 10.1007/s11604-009-0314-7]

114 **Baron P**, Dorrius MD, Kappert P, Oudkerk M, Sijens PE. Diffusion-weighted imaging of normal fibroglandular breast tissue: influence of microperfusion and fat suppression technique on the apparent diffusion coefficient. *NMR Biomed* 2010; **23**: 399-405 [PMID: 20131313 DOI: 10.1002/nbm.1475]

115 **Yablonskiy DA**, Sukstanskii AL. Theoretical models of the diffusion weighted MR signal. *NMR Biomed* 2010; **23**: 661-681 [PMID: 20886562 DOI: 10.1002/nbm.1520]

116 **Szafer A**, Zhong J, Anderson AW, Gore JC. Diffusion-weighted imaging in tissues: theoretical models. *NMR Biomed* 1995; **8**: 289-296 [PMID: 8739267]

117 **Sugahara T**, Korogi Y, Kochi M, Ikushima I, Shigematu Y, Hirai T, Okuda T, Liang L, Ge Y, Komohara Y, Ushio Y, Takahashi M. Usefulness of diffusion-weighted MRI with echo-planar technique in the evaluation of cellularity in gliomas. *J Magn Reson Imaging* 1999; **9**: 53-60 [PMID: 10030650 DOI: 10.1002/(SICI)1522-2586(199901)9:1<53::AID-JMRI7>3.0.CO;2-2]

118 **Guo Y**, Cai YQ, Cai ZL, Gao YG, An NY, Ma L, Mahankali S, Gao JH. Differentiation of clinically benign and malignant breast lesions using diffusion-weighted imaging. *J Magn Reson Imaging* 2002; **16**: 172-178 [PMID: 12203765 DOI: 10.1002/jmri.10140]

119 **Kim SH**, Cha ES, Kim HS, Kang BJ, Choi JJ, Jung JH, Park YG, Suh YJ. Diffusion-weighted imaging of breast cancer: correlation of the apparent diffusion coefficient value with prognostic factors. *J Magn Reson Imaging* 2009; **30**: 615-620 [PMID: 19711411 DOI: 10.1002/jmri.21884]

120 **Bharwani N**, Miquel ME, Sahdev A, Narayanan P, Malietzis G, Reznek RH, Rockall AG. Diffusion-weighted imaging in the assessment of tumour grade in endometrial cancer. *Br J Radiol* 2011; **84**: 997-1004 [PMID: 21896664 DOI: 10.1259/bjr/14980811]

121 **Watanabe Y**, Terai A, Araki T, Nagayama M, Okumura A, Amoh Y, Ishimori T, Ishibashi M, Nakashita S, Dodo Y. Detection and localization of prostate cancer with the targeted biopsy strategy based on ADC map: a prospective large-scale cohort study. *J Magn Reson Imaging* 2012; **35**: 1414-1421 [PMID: 22246980 DOI: 10.1002/jmri.23587]

122 **TISO**. Accuracy (trueness and precision) of measurement methods and results ISO5725. The International Organization for Standardization, 1994; 6: 41. Available from: URL: https://www.iso.org/obp/ui/#iso:std:iso:5725:-1:ed-1:v1:en

123 **Bland JM**, Altman DG. Statistical methods for assessing agreement between two methods of clinical measurement. *Lancet* 1986; **1**: 307-310 [PMID: 2868172 DOI: 10.1016/S0140-6736(86)90837-8]

124 **Raunig DL**, McShane LM, Pennello G, Gatsonis C, Carson PL, Voyvodic JT, Wahl RL, Kurland BF, Schwarz AJ, Gönen M, Zahlmann G, Kondratovich MV, O'Donnell K, Petrick N, Cole PE, Garra B, Sullivan DC. Quantitative imaging biomarkers: a review of statistical methods for technical performance assessment. *Stat Methods Med Res* 2015; **24**: 27-67 [PMID: 24919831 DOI: 10.1177/0962280214537344]

125 **Chenevert TL**, Galbán CJ, Ivancevic MK, Rohrer SE, Londy FJ, Kwee TC, Meyer CR, Johnson TD, Rehemtulla A, Ross BD. Diffusion coefficient measurement using a temperature-controlled fluid for quality control in multicenter studies. *J Magn Reson Imaging* 2011; **34**: 983-987 [PMID: 21928310 DOI: 10.1002/jmri.22363]

126 **Sasaki M**, Yamada K, Watanabe Y, Matsui M, Ida M, Fujiwara S, Shibata E. Variability in absolute apparent diffusion coefficient values across different platforms may be substantial: a multivendor, multi-institutional comparison study. *Radiology* 2008; **249**: 624-630 [PMID: 18936317 DOI: 10.1148/radiol.2492071681]

127 **Tofts PS**, Collins DJ. Multicentre imaging measurements for oncology and in the brain. *Br J Radiol* 2011; **84** Spec No 2: S213-S226 [PMID: 22433831 DOI: 10.1259/bjr/74316620]

128 **Sinkus R**, Van Beers BE, Vilgrain V, DeSouza N, Waterton JC. Apparent diffusion coefficient from magnetic resonance imaging as a biomarker in oncology drug development. *Eur J Cancer* 2012; **48**: 425-431 [PMID: 22226479 DOI: 10.1016/j.ejca.2011.11.034]

129 **Kim SY**, Lee SS, Byun JH, Park SH, Kim JK, Park B, Kim N, Lee MG. Malignant hepatic tumors: short-term reproducibility of apparent diffusion coefficients with breath-hold and respiratory-triggered diffusion-weighted MR imaging. *Radiology* 2010; **255**: 815-823 [PMID: 20501719 DOI: 10.1148/radiol.10091706]

130 **Tofts PS**. QA: Quality Assurance, Accuracy, Precision and Phantoms. In: Quantitative MRI of the Brain, 2004: 55-81 [DOI: 10.1002/0470869526.ch3]

131 **Tofts PS**, Lloyd D, Clark CA, Barker GJ, Parker GJ, McConville P, Baldock C, Pope JM. Test liquids for quantitative MRI measurements of self-diffusion coefficient in vivo. *Magn Reson Med* 2000; **43**: 368-374 [PMID: 10725879 DOI: 10.1002/(SICI)1522-2594(200003)43:3<368::AID-MRM8>3.0.CO;2-B]

132 **Holz M**, Heil SR, Sacco A. Temperature-dependent self-diffusion coefficients of water and six selected molecular liquids for calibration in accurate H-1 NMR PFG measurements. *Phys Chem Chem Phys* 2000; **2**: 4740-4742 [DOI: 10.1039/b005319h]

133 **Laubach HJ**, Jakob PM, Loevblad KO, Baird AE, Bovo MP, Edelman RR, Warach S. A phantom for diffusion-weighted imaging of acute stroke. *J Magn Reson Imaging* 1998; **8**: 1349-1354 [PMID: 9848751 DOI: 10.1002/jmri.1880080627]

134 **Delakis I**, Moore EM, Leach MO, De Wilde JP. Developing a quality control protocol for diffusion imaging on a clinical MRI system. *Phys Med Biol* 2004; **49**: 1409-1422 [PMID: 15152682 DOI: 10.1088/0031-9155/49/8/003]

135 **Lavdas I**, Behan KC, Papadaki A, McRobbie DW, Aboagye EO. A phantom for diffusion-weighted MRI (DW-MRI). *J Magn Reson Imaging* 2013; **38**: 173-179 [PMID: 23576443 DOI: 10.1002/jmri.23950]

136 **Lavdas I**, Miquel ME, McRobbie DW, Aboagye EO. Comparison between diffusion-weighted MRI (DW-MRI) at 1.5 and 3 tesla: a phantom study. *J Magn Reson Imaging* 2014; **40**: 682-690 [PMID: 24925470 DOI: 10.1002/jmri.24397]

137 **Malyarenko D**, Galbán CJ, Londy FJ, Meyer CR, Johnson TD, Rehemtulla A, Ross BD, Chenevert TL. Multi-system repeatability and reproducibility of apparent diffusion coefficient measurement using an ice-water phantom. *J Magn Reson Imaging* 2013; **37**: 1238-1246 [PMID: 23023785 DOI: 10.1002/jmri.23825]

138 **Kıvrak AS**, Paksoy Y, Erol C, Koplay M, Özbek S, Kara F. Comparison of apparent diffusion coefficient values among different MRI platforms: a multicenter phantom study. *Diagn Interv Radiol* 2013; **19**: 433-437 [PMID: 24004973 DOI: 10.5152/dir.2013.13034]

139 **Giannelli M**, Sghedoni R, Iacconi C, Iori M, Traino AC, Guerrisi M, Mascalchi M, Toschi N, Diciotti S. MR scanner systems should be adequately characterized in diffusion-MRI of the breast. *PLoS One* 2014; **9**: e86280 [PMID: 24489711 DOI: 10.1371/journal.pone.0086280]

140 **Belli G**, Busoni S, Ciccarone A, Coniglio A, Esposito M, Giannelli M, Mazzoni LN, Nocetti L, Sghedoni R, Tarducci R, Zatelli G, Anoja RA, Belmonte G, Bertolino N, Betti M, Biagini C, Ciarmatori A, Cretti F, Fabbri E, Fedeli L, Filice S, Fulcheri CP, Gasperi C, Mangili PA, Mazzocchi S, Meliadò G, Morzenti S, Noferini L, Oberhofer N, Orsingher L, Paruccini N, Principalli G, Quattrocchi M, Rinaldi A, Scelfo D, Freixas GV, Tenori L, Zucca I, Luchinat C, Gori C, Gobbi G, Italian Association of Physics in Medicine (AIFM) Working Group on MRIntercomparison. Quality assurance multicenter comparison of different MR scanners for quantitative diffusion-weighted imaging. *J Magn Reson Imaging* 2015; Epub ahead of print [PMID: 26013043 DOI: 10.1002/jmri.24956]

141 **Doblas S**, Almeida GS, Blé FX, Garteiser P, Hoff BA, McIntyre DJ, Wachsmuth L, Chenevert TL, Faber C, Griffiths JR, Jacobs AH, Morris DM, O'Connor JP, Robinson SP, Van Beers BE, Waterton JC. Apparent diffusion coefficient is highly reproducible on preclinical imaging systems: Evidence from a seven-center multivendor study. *J Magn Reson Imaging* 2015; Epub ahead of print [PMID: 26012876 DOI: 10.1002/jmri.24955]

142 **Colagrande S**, Pasquinelli F, Mazzoni LN, Belli G, Virgili G. MR-diffusion weighted imaging of healthy liver parenchyma: repeatability and reproducibility of apparent diffusion coefficient measurement. *J Magn Reson Imaging* 2010; **31**: 912-920 [PMID: 20373436 DOI: 10.1002/jmri.22117]

143 **Bilgili MY**. Reproductibility of apparent diffusion coefficients measurements in diffusion-weighted MRI of the abdomen with different b values. *Eur J Radiol* 2012; **81**: 2066-2068 [PMID: 21724354 DOI: 10.1016/j.ejrad.2011.06.045]

144 **Chen X**, Qin L, Pan D, Huang Y, Yan L, Wang G, Liu Y, Liang C, Liu Z. Liver diffusion-weighted MR imaging: reproducibility comparison of ADC measurements obtained with multiple breath-hold, free-breathing, respiratory-triggered, and navigator-triggered techniques. *Radiology* 2014; **271**: 113-125 [PMID: 24475860 DOI: 10.1148/radiol.13131572]

145 **Jajamovich GH**, Dyvorne H, Donnerhack C, Taouli B. Quantitative liver MRI combining phase contrast imaging, elastography, and DWI: assessment of reproducibility and postprandial effect at 3.0 T. *PLoS One* 2014; **9**: e97355 [PMID: 24840288 DOI: 10.1371/journal.pone.0097355]

146 **Pazahr S**, Nanz D, Rossi C, Chuck N, Stenger I, Wurnig MC, Schick F, Boss A. Magnetic resonance imaging of the liver: apparent diffusion coefficients from multiexponential analysis of b values greater than 50 s/mm2 do not respond to caloric intake despite increased portal-venous blood flow. *Invest Radiol* 2014; **49**: 138-146 [PMID: 24169068 DOI: 10.1097/RLI.0000000000000005]

147 **Kolff-Gart AS**, Pouwels PJ, Noij DP, Ljumanovic R, Vandecaveye V, de Keyzer F, de Bree R, de Graaf P, Knol DL, Castelijns JA. Diffusion-weighted imaging of the head and neck in healthy subjects: reproducibility of ADC values in different MRI systems and repeat sessions. *AJNR Am J Neuroradiol* 2015; **36**: 384-390 [PMID: 25258365 DOI: 10.3174/ajnr.A4114]

148 **Grech-Sollars M**, Hales PW, Miyazaki K, Raschke F, Rodriguez D, Wilson M, Gill SK, Banks T, Saunders DE, Clayden JD, Gwilliam MN, Barrick TR, Morgan PS, Davies NP, Rossiter J, Auer DP, Grundy R, Leach MO, Howe FA, Peet AC, Clark CA. Multi-centre reproducibility of diffusion MRI parameters for clinical sequences in the brain. *NMR Biomed* 2015; **28**: 468-485 [PMID: 25802212 DOI: 10.1002/nbm.3269]

149 **Winfield JM**, Papoutsaki MV, Ragheb H, Morris DM, Heerschap A, ter Voert EG, Kuijer JP, Pieters IC, Douglas NH, Orton M, de Souza NM. Development of a diffusion-weighted MRI protocol for multicentre abdominal imaging and evaluation of the effects of fasting on measurement of apparent diffusion coefficients (ADCs) in healthy liver. *Br J Radiol* 2015; **88**: 20140717 [PMID: 25790061 DOI: 10.1259/bjr.20140717]

150 **Malyarenko DI**, Newitt D, J. Wilmes L, Tudorica A, Helmer KG, Arlinghaus LR, Jacobs MA, Jajamovich G, Taouli B, Yankeelov TE, Huang W, Chenevert TL. Demonstration of nonlinearity bias in the measurement of the apparent diffusion coefficient in multicenter trials. *Magn Reson Med* 2015; Epub ahead of print [PMID: 25940607 DOI: 10.1002/mrm.25754]

151 **Winfield JM**, deSouza NM, Priest AN, Wakefield JC, Hodgkin C, Freeman S, Orton MR, Collins DJ. Modelling DW-MRI data from primary and metastatic ovarian tumours. *Eur Radiol* 2015; **25**: 2033-2040 [PMID: 25605133 DOI: 10.1007/s00330-014-3573-3]

152 **Dickinson L**, Ahmed HU, Allen C, Barentsz JO, Carey B, Futterer JJ, Heijmink SW, Hoskin PJ, Kirkham A, Padhani AR, Persad R, Puech P, Punwani S, Sohaib AS, Tombal B, Villers A, van der Meulen J, Emberton M. Magnetic resonance imaging for the detection, localisation, and characterisation of prostate cancer: recommendations from a European consensus meeting. *Eur Urol* 2011; **59**: 477-494 [PMID: 21195536 DOI: 10.1016/j.eururo.2010.12.009]

153 **Ma C**, Liu L, Li J, Wang L, Chen LG, Zhang Y, Chen SY, Lu JP. Apparent diffusion coefficient (ADC) measurements in pancreatic adenocarcinoma: A preliminary study of the effect of region of interest on ADC values and interobserver variability. *J Magn Reson Imaging* 2015; Epub ahead of print [PMID: 26182908 DOI: 10.1002/jmri.25007]

154 **Koh DM**, Blackledge M, Collins DJ, Padhani AR, Wallace T, Wilton B, Taylor NJ, Stirling JJ, Sinha R, Walicke P, Leach MO, Judson I, Nathan P. Reproducibility and changes in the apparent diffusion coefficients of solid tumours treated with combretastatin A4 phosphate and bevacizumab in a two-centre phase I clinical trial. *Eur Radiol* 2009; **19**: 2728-2738 [PMID: 19547986 DOI: 10.1007/s00330-009-1469-4]

155 **Boulanger Y**, Amara M, Lepanto L, Beaudoin G, Nguyen BN, Allaire G, Poliquin M, Nicolet V. Diffusion-weighted MR imaging of the liver of hepatitis C patients. *NMR Biomed* 2003; **16**: 132-136 [PMID: 12884356 DOI: 10.1002/nbm.818]

156 **Deng J**, Miller FH, Salem R, Omary RA, Larson AC. Multishot diffusion-weighted PROPELLER magnetic resonance imaging of the abdomen. *Invest Radiol* 2006; **41**: 769-775 [PMID: 16971801 DOI: 10.1097/01.rli.0000236808.84746.95]

157 **Lewin M**, Poujol-Robert A, Boëlle PY, Wendum D, Lasnier E, Viallon M, Guéchot J, Hoeffel C, Arrivé L, Tubiana JM, Poupon R. Diffusion-weighted magnetic resonance imaging for the assessment of fibrosis in chronic hepatitis C. *Hepatology* 2007; **46**: 658-665 [PMID: 17663420 DOI: 10.1002/hep.21747]

158 **Taouli B**, Tolia AJ, Losada M, Babb JS, Chan ES, Bannan MA, Tobias H. Diffusion-weighted MRI for quantification of liver fibrosis: preliminary experience. *AJR Am J Roentgenol* 2007; **189**: 799-806 [PMID: 17885048 DOI: 10.2214/AJR.07.2086]

159 **Luciani A**, Vignaud A, Cavet M, Nhieu JT, Mallat A, Ruel L, Laurent A, Deux JF, Brugieres P, Rahmouni A. Liver cirrhosis: intravoxel incoherent motion MR imaging--pilot study. *Radiology* 2008; **249**: 891-899 [PMID: 19011186 DOI: 10.1148/radiol.2493080080]

160 **Bruegel M**, Holzapfel K, Gaa J, Woertler K, Waldt S, Kiefer B, Stemmer A, Ganter C, Rummeny EJ. Characterization of focal liver lesions by ADC measurements using a respiratory triggered diffusion-weighted single-shot echo-planar MR imaging technique. *Eur Radiol* 2008; **18**: 477-485 [PMID: 17960390 DOI: 10.1007/s00330-007-0785-9]

161 **Saremi F**, Jalili M, Sefidbakht S, Channual S, Quane L, Naderi N, Schultze-Haakh H, Torrone M. Diffusion-weighted imaging of the abdomen at 3 T: image quality comparison with 1.5-T magnet using 3 different imaging sequences. *J Comput Assist Tomogr* 2011; **35**: 317-325 [PMID: 21586923 DOI: 10.1097/RCT.0b013e318213ccb0]

162 **Bakan AA**, Inci E, Bakan S, Gokturk S, Cimilli T. Utility of diffusion-weighted imaging in the evaluation of liver fibrosis. *Eur Radiol* 2012; **22**: 682-687 [PMID: 21984447 DOI: 10.1007/s00330-011-2295-z]

163 **Andreou A**, Koh DM, Collins DJ, Blackledge M, Wallace T, Leach MO, Orton MR. Measurement reproducibility of perfusion fraction and pseudodiffusion coefficient derived by intravoxel incoherent motion diffusion-weighted MR imaging in normal liver and metastases. *Eur Radiol* 2013; **23**: 428-434 [PMID: 23052642 DOI: 10.1007/s00330-012-2604-1]

164 **Penner AH**, Sprinkart AM, Kukuk GM, Gütgemann I, Gieseke J, Schild HH, Willinek WA, Mürtz P. Intravoxel incoherent motion model-based liver lesion characterisation from three b-value diffusion-weighted MRI. *Eur Radiol* 2013; **23**: 2773-2783 [PMID: 23666233 DOI: 10.1007/s00330-013-2869-z]

165 **Duran R**, Ronot M, Di Renzo S, Gregoli B, Van Beers BE, Vilgrain V. Is magnetic resonance imaging of hepatic hemangioma any different in liver fibrosis and cirrhosis compared to normal liver? *Eur J Radiol* 2015; **84**: 816-822 [PMID: 25703650 DOI: 10.1016/j.ejrad.2015.01.016]

166 **Sulkowska K**, Palczewski P, Duda-Zysk A, Szeszkowski W, Wojcik D, Kownacka-Piotrowska D, Gołębiowski M. Diffusion-weighted MRI of kidneys in healthy volunteers and living kidney donors. *Clin Radiol* 2015; **70**: 1122-1127 [PMID: 26149258 DOI: 10.1016/j.crad.2015.05.016]

167 **Thomas S**, Kayhan A, Lakadamyali H, Oto A. Diffusion MRI of acute pancreatitis and comparison with normal individuals using ADC values. *Emerg Radiol* 2012; **19**: 5-9 [PMID: 21927794 DOI: 10.1007/s10140-011-0983-2]

168 **Ma C**, Wang J, Li Y, Pan C, Zhang Y, Wang H, Chen SaLJ. Comparisons of Image Quality and ADCs in Breath-Hold, Respiratory-Triggered and Free-Breathing DWI of Pancreas at 3-T. *O J Rad* 2014; **4**: 279-292 [DOI: 10.4236/ojrad.2014.44037]

169 **Issa B**. In vivo measurement of the apparent diffusion coefficient in normal and malignant prostatic tissues using echo-planar imaging. *J Magn Reson Imaging* 2002; **16**: 196-200 [PMID: 12203768 DOI: 10.1002/jmri.10139]

170 **Pickles MD**, Gibbs P, Sreenivas M, Turnbull LW. Diffusion-weighted imaging of normal and malignant prostate tissue at 3.0T. *J Magn Reson Imaging* 2006; **23**: 130-134 [PMID: 16374882 DOI: 10.1002/jmri.20477]

171 **Gibbs P**, Pickles MD, Turnbull LW. Repeatability of echo-planar-based diffusion measurements of the human prostate at 3 T. *Magn Reson Imaging* 2007; **25**: 1423-1429 [PMID: 17499468 DOI: 10.1016/j.mri.2007.03.030]

172 **Ren J**, Huan Y, Wang H, Zhao H, Ge Y, Chang Y, Liu Y. Diffusion-weighted imaging in normal prostate and differential diagnosis of prostate diseases. *Abdom Imaging* 2008; **33**: 724-728 [PMID: 18219519 DOI: 10.1007/s00261-008-9361-2]

173 **Tamada T**, Sone T, Toshimitsu S, Imai S, Jo Y, Yoshida K, Yamamoto A, Yamashita T, Egashira N, Nagai K, Fukunaga M. Age-related and zonal anatomical changes of apparent diffusion coefficient values in normal human prostatic tissues. *J Magn Reson Imaging* 2008; **27**: 552-556 [PMID: 18219616 DOI: 10.1002/jmri.21117]

174 **Liu X**, Peng W, Zhou L, Wang H. Biexponential apparent diffusion coefficients values in the prostate: comparison among normal tissue, prostate cancer, benign prostatic hyperplasia and prostatitis. *Korean J Radiol* 2013; **14**: 222-232 [PMID: 23483254 DOI: 10.3348/kjr.2013.14.2.222]

175 **Peng Y**, Jiang Y, Antic T, Sethi I, Schmid-Tannwald C, Eggener S, Oto A. Apparent diffusion coefficient for prostate cancer imaging: impact of B values. *AJR Am J Roentgenol* 2014; **202**: W247-W253 [PMID: 24555621 DOI: 10.2214/AJR.13.10917]

176 **Zhang Y**, Liang BL, Gao L, Ye RX, Shen J, Zhong JL. [Diffusion weighted imaging features of normal uterine cervix and cervical carcinoma]. *Ai Zheng* 2007; **26**: 508-512 [PMID: 17672942 DOI: 1000-467X200705508]

177 **Fujii S**, Matsusue E, Kigawa J, Sato S, Kanasaki Y, Nakanishi J, Sugihara S, Kaminou T, Terakawa N, Ogawa T. Diagnostic accuracy of the apparent diffusion coefficient in differentiating benign from malignant uterine endometrial cavity lesions: initial results. *Eur Radiol* 2008; **18**: 384-389 [PMID: 17917730 DOI: 10.1007/s00330-007-0769-9]

178 **Inada Y**, Matsuki M, Nakai G, Tatsugami F, Tanikake M, Narabayashi I, Yamada T, Tsuji M. Body diffusion-weighted MR imaging of uterine endometrial cancer: is it helpful in the detection of cancer in nonenhanced MR imaging? *Eur J Radiol* 2009; **70**: 122-127 [PMID: 18182265 DOI: 10.1016/j.ejrad.2007.11.042]

179 **Liu Y**, Bai R, Sun H, Liu H, Wang D. Diffusion-weighted magnetic resonance imaging of uterine cervical cancer. *J Comput Assist Tomogr* 2009; **33**: 858-862 [PMID: 19940650 DOI: 10.1097/RCT.0b013e31819e93af]

180 **Payne GS**, Schmidt M, Morgan VA, Giles S, Bridges J, Ind T, DeSouza NM. Evaluation of magnetic resonance diffusion and spectroscopy measurements as predictive biomarkers in stage 1 cervical cancer. *Gynecol Oncol* 2010; **116**: 246-252 [PMID: 19875159 DOI: 10.1016/j.ygyno.2009.09.044]

181 **Englander SA**, Uluğ AM, Brem R, Glickson JD, van Zijl PC. Diffusion imaging of human breast. *NMR Biomed* 1997; **10**: 348-352 [PMID: 9471126 DOI: 10.1002/(SICI)1099-1492(199710)10:7<348::AID-NBM487>3.0.CO;2-R]

182 **Park MJ**, Cha ES, Kang BJ, Ihn YK, Baik JH. The role of diffusion-weighted imaging and the apparent diffusion coefficient (ADC) values for breast tumors. *Korean J Radiol* 2007; **8**: 390-396 [PMID: 17923781 DOI: 10.3348/kjr.2007.8.5.390]

183 **Tagliafico A**, Rescinito G, Monetti F, Villa A, Chiesa F, Fisci E, Pace D, Calabrese M. Diffusion tensor magnetic resonance imaging of the normal breast: reproducibility of DTI-derived fractional anisotropy and apparent diffusion coefficient at 3.0 T. *Radiol Med* 2012; **117**: 992-1003 [PMID: 22580812 DOI: 10.1007/s11547-012-0831-9]

184 **McDonald ES**, Schopp JG, Peacock S, DeMartini WB, Rahbar H, Lehman CD, Partridge SC. Diffusion-weighted MRI: association between patient characteristics and apparent diffusion coefficients of normal breast fibroglandular tissue at 3 T. *AJR Am J Roentgenol* 2014; **202**: W496-W502 [PMID: 24758685 DOI: 10.2214/

AJR.13.11159]

185 **Sugita R**, Yamazaki T, Furuta A, Itoh K, Fujita N, Takahashi S. High b-value diffusion-weighted MRI for detecting gallbladder carcinoma: preliminary study and results. *Eur Radiol* 2009; **19**: 1794-1798 [PMID: 19190910 DOI: 10.1007/s00330-009-1322-9]

186 **Taouli B**, Thakur RK, Mannelli L, Babb JS, Kim S, Hecht EM, Lee VS, Israel GM. Renal lesions: characterization with diffusion-weighted imaging versus contrast-enhanced MR imaging. *Radiology* 2009; **251**: 398-407 [PMID: 19276322 DOI: 10.1148/radiol.2512080880]

187 **Wang H**, Cheng L, Zhang X, Wang D, Guo A, Gao Y, Ye H. Renal cell carcinoma: diffusion-weighted MR imaging for subtype differentiation at 3.0 T. *Radiology* 2010; **257**: 135-143 [PMID: 20713607 DOI: 10.1148/radiol.10092396]

188 **Ogawa T**, Horaguchi J, Fujita N, Noda Y, Kobayashi G, Ito K, Koshita S, Kanno Y, Masu K, Sugita R. High b-value diffusion-weighted magnetic resonance imaging for gallbladder lesions: differentiation between benignity and malignancy. *J Gastroenterol* 2012; **47**: 1352-1360 [PMID: 22576026 DOI: 10.1007/s00535-012-0604-1]

P- Reviewer: Strigari L, Wang YXJ
S- Editor: Ji FF **L- Editor**: A **E- Editor**: Li D

Published by **Baishideng Publishing Group Inc**
8226 Regency Drive, Pleasanton, CA 94588, USA
Telephone: +1-925-223-8242
Fax: +1-925-223-8243
E-mail: bpgoffice@wjgnet.com
Help Desk: http://www.wjgnet.com/esps/helpdesk.aspx
http://www.wjgnet.com